JOURNAL OF GEOPHYSICAL RESEARCH, VOL. 106, NO. E10, PAGES 23,291–23,316, OCTOBER 25, 2001

Overview of the Mars Global Surveyor mission

Arden L. Albee
Division of Geological and Planetary Sciences, California Institute of Technology, Pasadena, California

Raymond E. Arvidson
McDonnell Center for the Space Sciences, Department of Earth and Planetary Sciences
Washington University, St. Louis, Missouri

Frank Palluconi and Thomas Thorpe
Jet Propulsion Laboratory, Pasadena, California

Abstract. The Mars Global Surveyor spacecraft was placed into Mars orbit on September 11, 1997, and by March 9, 1999, had slowly circularized through aerobraking to a Sun-synchronous, near-polar orbit with an average altitude of 378 km. The science payload includes the Mars Orbiter Camera, Mars Orbiter Laser Altimeter, Thermal Emission Spectrometer, Ultrastable Oscillator (for Radio Science experiments), and Magnetometer/Electron Reflectometer package. In addition, the spacecraft accelerometers and horizon sensors were used to study atmospheric dynamics during aerobraking. Observations are processed to standard products by the instrument teams and released as documented archive volumes on 6-month centers by the Planetary Data System. Significant results have been obtained from observations of the interior, surface, and atmosphere. For example, Mars does not now have an active magnetic field, although strong remanent magnetization features exist in the ancient crust. These results imply that an internal dynamo ceased operation early in geologic time. Altimetry and gravity data indicate that the crust is thickest under the south pole, thinning northward from the cratered terrain to the northern plains. Analysis of altimetry data demonstrates that Mars is "egg-shaped" with gravitational equipotential contours that show that channel systems in the southern highlands drained to the north, largely to the Chryse trough. A closed contour in the northern plains is consistent with the existence of a great northern ocean. Emission spectra of low-albedo regions show that basaltic rocks dominate spectral signatures on the southern highlands, whereas basaltic andesites dominate the northern lowlands. The bright regions show nondiagnostic spectra, similar to that of dust in the atmosphere. Signatures of aqueous minerals (e.g., clays, carbonates, and sulfates) are noticeably absent from the emission spectra. High spatial resolution images show that the surface has been extensively modified by wind and that layering is nearly ubiquitous, implying that a complex history of events is recorded in surface and near-surface materials. Altimetry data imply that both permanent caps are composed of water ice and dust, with seasonal covers of carbon dioxide frost. Finally, the altimetry data, coupled with thousands of atmospheric profiles, are providing new boundary conditions and dynamic controls for the generation and testing of more realistic dynamic models of the global circulation of the atmosphere.

1. Introduction

Observations from the two orbiters and two landers that were part of the 1976 Viking mission demonstrated that Mars' history is complex both geologically and climatically and that the current environment and climate are both dynamic [*Kieffer et al.*, 1992]. Perhaps as many questions were raised about Mars as were answered through analyses of Viking data. Issues included the origin and history of the putative fluvial and lacustrine landforms, the composition and mineralogy of the major crustal units, the composition and dynamics of the polar caps, and a myriad of questions associated with atmospheric circulation. By the early 1980s it was clear that the next mission to explore Mars should be an orbiter to obtain a complementary suite of observations of the atmosphere, surface, and interior for a full Mars year from a near-circular, Sun-synchronous orbit. The Mars Observer (MO) mission was developed to conduct these global studies [*Albee et al.*, 1992]. Unfortunately, that spacecraft was lost in August 1993, just as it approached Mars orbit insertion.

Mars Global Surveyor (MGS) is the first mission conducted under the auspices of the NASA Mars Surveyor Program. This program has as its foci understanding the current and past climates of Mars, whether or not life started and evolved on the Red Planet, and the geological and geophysical evolution of the planet. The history and current state of water are integrating themes for the program. MGS utilized spare components, science instruments, and designs from Mars Observer in a configuration only about half the size of the Observer spacecraft. Further, MGS was launched on a Delta as opposed to the

Paper number 2000JE001306.
0148-0227/01/2000JE001306$09.00

larger Titan rocket. As a result, the two heaviest instruments from Mars Observer are slated to fly on later missions in the program.

The formal science objectives for the MGS mission are to (1) characterize surface morphology at high spatial resolution to quantify surface characteristics and geological processes, (2) determine the composition and map the distribution of surface minerals, rocks, and ices and measure surface thermophysical properties, (3) determine globally the topography, geodetic figure, and gravitational field, (4) establish the nature of the magnetic field and map the crustal remnant field, (5) monitor global weather and thermal structure of the atmosphere, and (6) study surface-atmosphere interaction by monitoring surface features, polar caps, polar thermal balance, atmospheric dust, and condensate clouds over a seasonal cycle.

These objectives and the basic mission design are consistent with the Mars Surveyor Program themes and the earlier recommendations of the *Solar System Exploration Committee* [1983]. Several other objectives have been adopted for the MGS Mission as part of its inclusion in the Mars Surveyor Program: (1) provide multiple years of on-orbit relay communications capability for Mars landers and atmospheric vehicles from any nation interested in participating in the International Mars Surveyor Program and (2) support landing site selection planning for future Mars Surveyor Program missions through acquisition of high-resolution imaging and other relevant data sets.

In this paper an overview of the MGS Mission and its major accomplishments to date are presented. Subsequent papers in this issue provide detailed results from analyses of key measurements from the instruments aboard the spacecraft.

2. Mission Design

The science objectives for MGS presented a number of challenges for the mission design. The spacecraft, instruments, communications, ground data system, and required orbit had to be designed to permit a logically integrated payload of science instruments to acquire high-quality, global observations of Mars' atmosphere, surface, and interior over an entire Mars year (687 days). Further, the data would need to be processed and distributed in a timely fashion for analysis by the collective planetary community. These overarching goals required finding a configuration that allowed all instruments to be operated simultaneously and continuously in the mapping orbit while data were transmitted to Earth and the solar panels maintained Sun-orientation to provide power.

Designing a specific mapping orbit to fulfill the science objectives, the extended radio relay period, and the Mars planetary protection requirements required meeting many constraints. In turn, the design of the mapping orbit placed significant constraints on the design of the spacecraft and the instruments. In general, these constraints were met by a low-altitude, near-circular, near-polar, Sun-synchronous orbit with a short repeat cycle (Table 1). The chosen combination resulted in a "frozen" orbit with a period of 117.65 min and an 88-revolution near-repeat cycle of ~7 sols (Martian days). The index altitude of 378 km is a measure of the difference between the semimajor axis length from the center of mass and a mean equatorial radius of Mars (3394.2 km). The height of the spacecraft above the "actual" surface of Mars ranges between 368 and 438 km. This frozen orbit essentially balances the secular motion of the argument of periapsis due to J2 by the variation due to the J3 component of the gravity field, thereby providing more stable spacecraft operation over an extended period [*Uphoff*, 1984]. The 88-revolution near-repeat pattern results in ground tracks spaced ~242 km apart at the equator at the end of 7 days (Figure 1). Each successive cycle fills in the spacing and under ideal conditions would result in 26 global cycles and a spacing of ~3 km at the equator at the end of the 2-year mapping mission. The Sun synchronicity was chosen as 1400/0200 LT, relative to the mean Sun position, to balance the requirements of the various instruments. The Mars Orbiter Camera (MOC) Team preferred late afternoon for distinctive shadows in the images, whereas the Thermal Emission Spectrometer (TES) Team preferred an orbit closer to 1300 LT, where higher ground temperature would result in a higher signal-to-noise ratio. However, the true Sun position actually varies during the course of the mission from nearly an hour ahead to nearly an hour behind the mean 1400 LT Sun position.

Table 1. MGS Mapping Orbit Characteristics

Characteristic	Attribute
Nodal period	117.65 min
Index altitude	378 km
Altitude above surface	368–438 km
Semimajor axis	3775.2 km
Inclination	92.96°
Eccentricity	0.01
Sun synchronous	1400/0200 LT (relative to mean Sun)
Earth to Mars range	0.578 AU (minimum on May 2, 2000) 1.666 AU (maximum on July 21, 2000)
Solar conjunction	July 1, 2000

During the mapping orbit configuration at Mars the spacecraft is continuously nadir-pointed, rotating at the orbital rate, as the high-gain antenna tracks Earth and the solar arrays track the Sun. The instruments are mounted on the nadir platform, permitting the use of simple, fixed, line-scan instruments, each with its own computer and without moving parts. This configuration, along with adequate data storage, downlink rate, and power margins, makes it possible for all instruments, including radio science, to be operated simultaneously and continuously with a single 10-hour pass per day on a 34-m Deep Space Station (DSN) ground station.

The use of chemical propulsion to reach the required mapping orbit would require a large mass of fuel, far beyond the injection capability of the Delta II launch vehicle. Therefore the spacecraft was designed to facilitate the use of aerobraking to attain the mapping orbit (Figure 2). After Mars orbital insertion, aerobraking utilizes repeated dips into the upper atmosphere using the atmospheric drag on the spacecraft to slow it so as to reach the low-altitude circular mapping orbit. Such a period of aerobraking had not been incorporated into the architecture of any previous mission, and the challenge was made more difficult by lack of knowledge of the structure and dynamics of the Mars atmosphere, especially at the aerobraking altitude.

3. Spacecraft Description and Configurations

The MGS spacecraft was designed to carry the science payload to Mars, place it into the desired mapping orbit with the use of aerobraking, maintain its proper pointing and orbit as a three-axis stabilized platform for acquiring mapping data, and

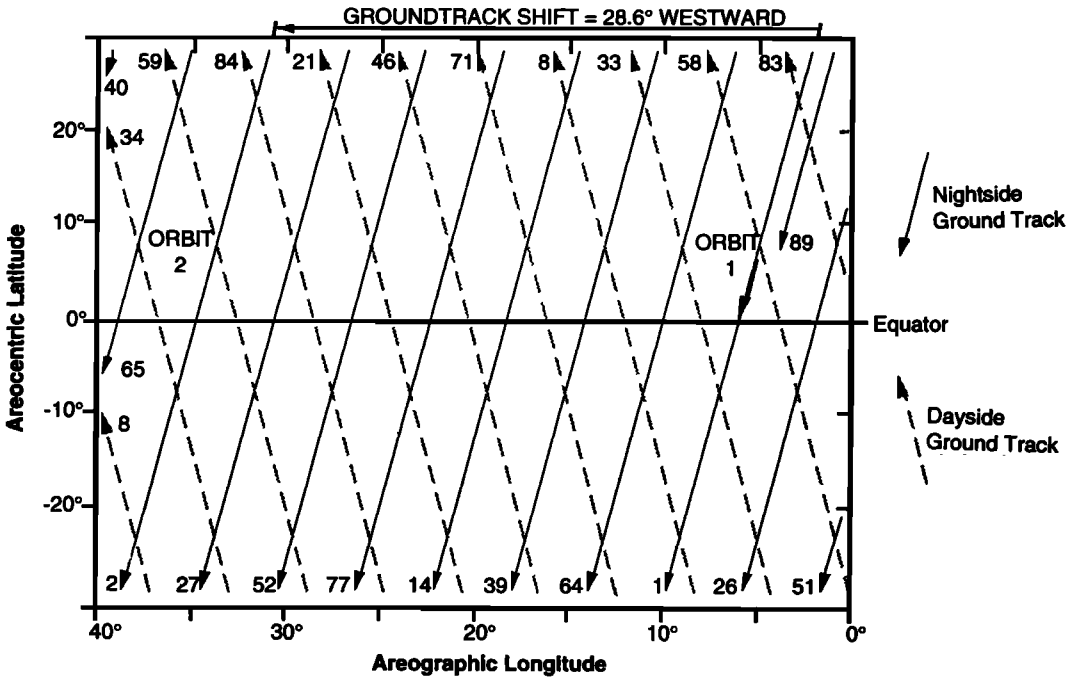

Figure 1. Mapping orbit ground track for 7-sol repeat cycle. The dashed lines are dayside ground tracks, and the solid lines are nightside ground tracks.

return the acquired data to Earth. The spacecraft's design, especially the electronic architecture, is based on that of Mars Observer [*Albee et al.*, 1992; *Cunningham*, 1995]. Most of the major electronic assemblies are spare Mars Observer units that have been retrofitted to eliminate any identified discrepancies. The design is generally single-fault tolerant with redundancy managed by central computers.

Lockheed Martin Astronautics (LMA), Denver, Colorado, built the spacecraft (Figure 3). In order to meet the stringent mass requirements, the spacecraft structure was constructed of lightweight composite material. It was divided into four subassemblies: the equipment module, the propulsion module, the solar array support structure, and the high-gain antenna (HGA) support structure. The equipment module houses the avionics packages and science instruments. Its dimensions are $1.221 \times 1.221 \times 0.762$ m in X, Y, and Z, respectively. With the exception of the Magnetometer/Electron Reflectometer, all of the science instruments are bolted to the nadir equipment deck, mounted above the equipment module on the $+Z$ panel. The Mars Relay antenna is the tallest instrument, extending 1.115 m above the nadir equipment deck (Figure 3).

The propulsion module serves as the adapter with the launch vehicle, contains the propellant tanks, main engine, and propulsion feed systems, and has the attitude control thrusters mounted on the four corners of the module. Two solar arrays, each 3.531×1.854 m, provide power. Including the structure that holds the array to the propulsion module, each panel extends 4.270 m from the side of the spacecraft in a Y direction and is further extended by a 0.813-m spring-mounted flap that was added to increase the ballistic coefficient during aerobraking and maintain the heating rate below 0.38 W/m^2. The two magnetometer sensors are mounted on the end of each array between the array and the flap (Figure 3). When fully deployed, the 1.5-m-diameter HGA sits on the end of a 2.0-m boom mounted to the $+X$ panel of the propulsion module.

As shown in Figure 4, the spacecraft assumes five different major configurations during various phases of the mission. In the launch configuration all of the appendages are in stowed position and fixed to the body of the spacecraft. During cruise the solar panels were deployed, whereas the HGA antenna was not. The HGA was pointed toward Earth, and the spacecraft rotates slowly about that axis, the array normal spin configuration. During aerobraking, as shown in Figure 4, the solar panels were swept back toward the payload so that the engine faced into the flow. During propulsive maneuvers the configuration was similar, but the solar panels were swept back toward the propulsion module. In the mapping configuration the spacecraft is three-axis controlled using input from the horizon sensor to keep the instruments pointing toward nadir. Gimbal drives enable the solar panels to track the Sun and enable the deployed HGA to track Earth. In safe and contingency modes the spacecraft locates the Sun and then cones at one revolution per hundred minutes about the Sun vector until contact with Earth is reestablished.

3.1. Command and Data Handling

The command and data-handling system is built around two redundant flight computers that run in parallel. The system consists of spare MO hardware with the exception of two solid state recorders (1.5 Gbits each) that replaced the three MO tape recorders for recording science and engineering data. Software resides in two redundant Marconi 1750A flight computers (128 Kwords RAM, 20 Kwords PROM): one in the engineering data formatter and one in the Payload Data System (PDS). The software in the flight computers controls almost all the spacecraft activities. While one computer is in active control, identical software runs concurrently in the backup unit. The flight software functions include attitude and articulation control, command processing, some telemetry functions, power management and battery charge control,

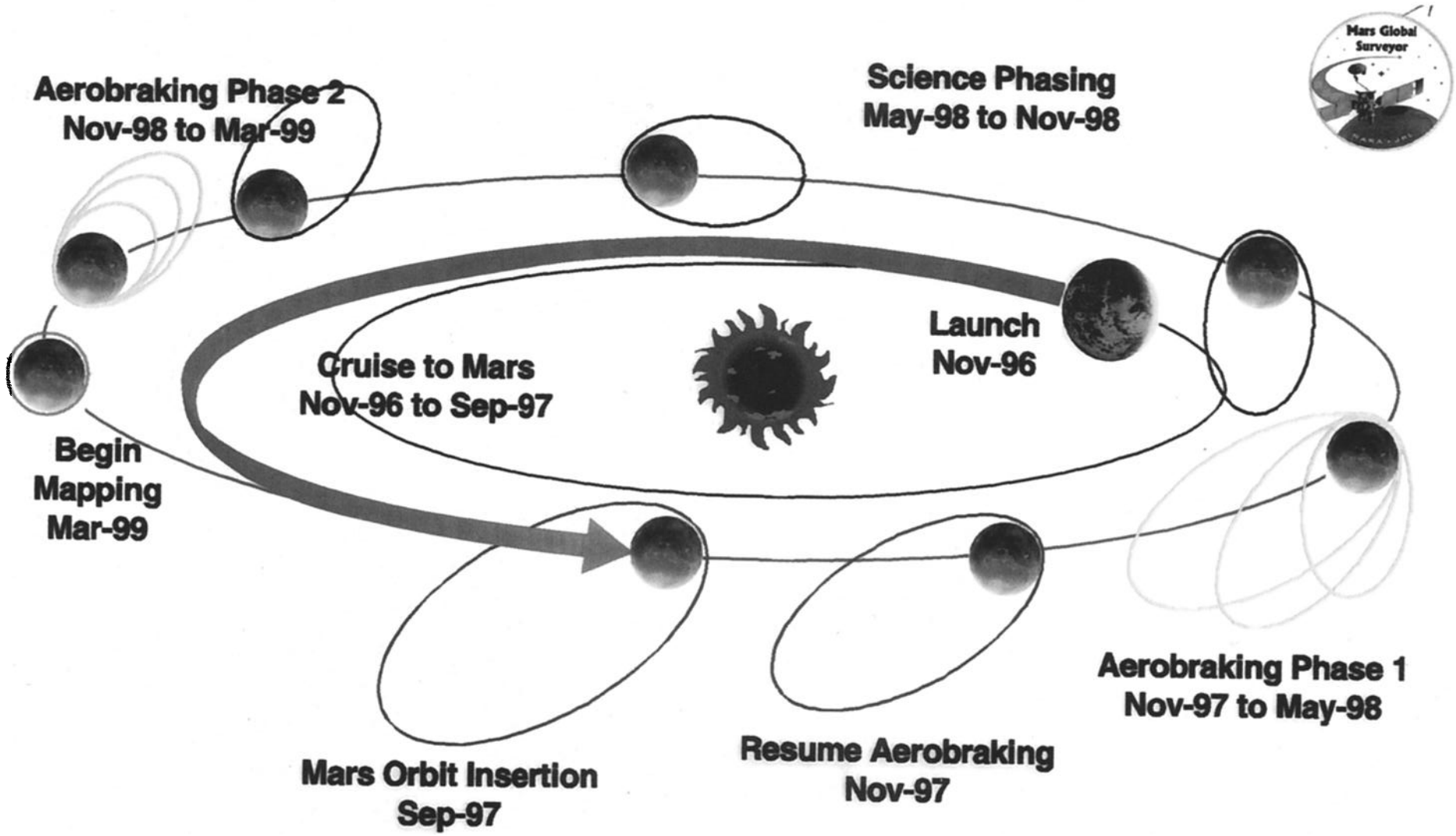

Figure 2. Summary of key MGS mission phases from launch to Mars orbit insertion in an elliptical orbit, initial aerobraking period, science-phasing period, aerobraking resumption, and mapping in the circular orbit.

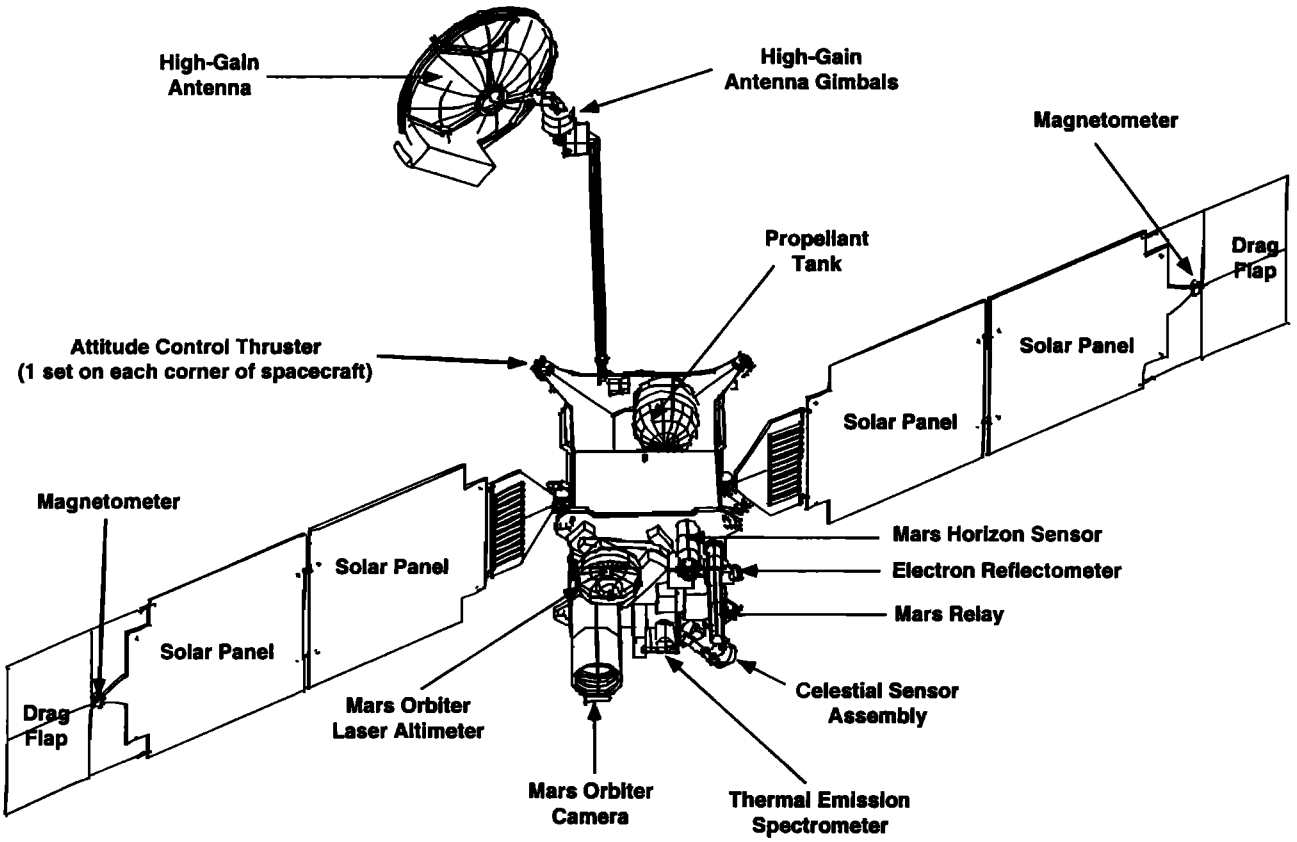

Figure 3. View of the MGS spacecraft showing major components and instruments.

thermal monitoring and heater control, and fault protection initiation and execution. Three levels of basic fault protection modes are utilized.

There are three different types of data streams and, because of the range in Earth-Mars distance, each can be returned at three different data rates. Instrument data and engineering data are collected in discrete packets with identification and timing information in a regular schedule unique to each data mode. The PDS collects the packets, formats the data into transfer frames, and Reed-Solomon encodes the transfer frames before storage in the recorder. The spacecraft then applies convolutional encoding prior to transmission by the radio system. Reed-Solomon encoding requires 1.147 bits (equals one symbol per second (sps)) to encode one bit of raw data.

S&E1 is a combined science and engineering data stream that can be recorded for later playback or played back in real time at rates of 4, 8, or 16 Ksps. S&E1 data are played back at a rate 5.333 times faster than the record rate, enabling the spacecraft to return 24 hours of recorded data during the dayside portion of the orbit in a single 10-hour DSN tracking pass. S&E2 is a combined science and engineering data stream that returns data only in real time at rates of 40 or 80 Ksps. ENG is a low-rate engineering-only data stream that can be recorded, played back in real time, or both. The bit allocations for the instruments differ with the various data streams and rates in order to ensure that all instruments can be operated simultaneously during the various phases of the mission. Two solid-state data recorders provide redundancy. Each consists of two 0.75-Gbit recorders that support simultaneous record and playback. Each unit can store up to 104 hours of data at the 4-Ksps record rate and over 26 hours at the 16-Ksps rate.

3.2. Attitude Control

Three-axis pointing control is provided through four reaction wheels. Attitude information is provided by a Mars horizon sensor that defines the nadir direction, a star tracker for inertial attitude, gyros and accelerometers for measuring angular rates and linear accelerations, and multiple Sun sensors. Three reaction wheels are mounted parallel to the three spacecraft axes; the fourth wheel is skewed to the others to provide backup redundancy. On January 18, 2001, the skew wheel was brought into use after an electrical failure in the x wheel controls. The spacecraft attitude is controlled to high precision by transferring momentum to and from the rapidly spinning reaction wheels. Sun sensors are placed at several locations about the spacecraft. Their primary use is during attitude reinitialization after a spacecraft anomaly. Data from these sensors are sufficient to characterize nadir and HGA pointing to within ± 3 mrad (per axis, 3 sigma).

3.3. Telecommunications and DSN Utilization

The X band (8.4 GHz) telecommunications system consists of two MO transponders, two Thompson 25-W traveling-wave tube power amplifiers, the 1.5-m MO high-gain antenna mounted on a 2-m boom, and four low-gain antennas (two for receive, two for transmit). The frequency modulator (RF) feed of the HGA was modified to accommodate a Ka band engineering experiment (REF) in which X band is converted to 32 GHz and amplified to ~0.5 W. The X band transponders are

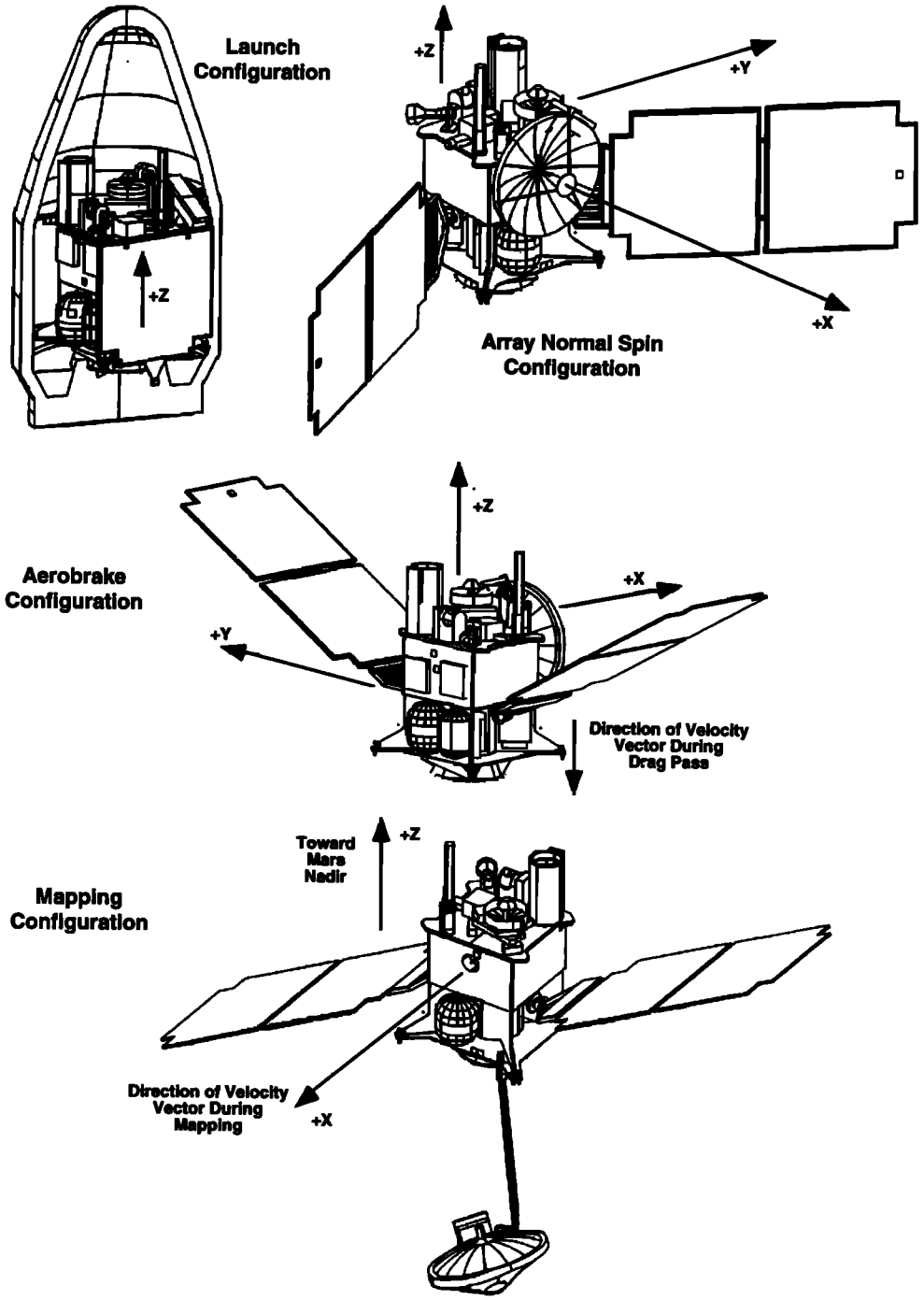

Figure 4. MGS spacecraft configurations for different phases of the mission (drag flaps are not shown; see Figure 3). During mapping the spacecraft is being flown in the minus X direction to accommodate the 1-year delay in achieving the mapping orbit.

in the main spacecraft structure, but the power amplifiers and the Ka band electronics are located in an enclosure on the back of the HGA. When deployed during mapping, two rotating joints (gimbals) allow the HGA to track and point to Earth while the science instruments observe Mars. The HGA was used in its position fixed to the spacecraft Y axis during cruise and aerobraking because it could not be deployed until all the burns of the main engine had been completed. Command sequences sent by the flight operations team on Earth flow to MGS at rates in multiples of 2 from 7.8125 bits/s (emergency rate) to 500 bits/s (750 commands per minute); the nominal rate is 125 bits/s. Downlink data rates are as high as 85333 bits/s when the Earth-Mars distance is small.

The 34-m high-efficiency (34mHEF) antennas of the DSN provide most of the tracking coverage for MGS because they have the capability to both transmit and receive X band signals. During normal operations in cruise, MGS operated with one 10-hour track per day, and an additional real-time 10-hour pass about every third day was added during the mapping period. During critical operations, including launch, maneuvers, and

Table 2. Characteristics of Mars Global Surveyor Instruments

Instrument Name	Description	Mass, kg	Power, W (Average Peak)	Data Rates, bits/s
Mars Orbiter Camera (MOC)	imaging: narrow and wide fields of view, 3.5-m focal length, 0.5–0.9 μm 11.4-mm focal length for blue and 11.0 mm for red (0.04–0.45 and 0.58–0.62 μm)	21.4	13.5/18.3	700/2,856/9,120 record 29,260/ 63,808 real time
Thermal Emission Spectrometer (TES)	interferometer with 6- to 50-μm spectral range and broad bands with 0.3–3.0 and 6–100 μm band passes	14.6	12.3/18.2	1,104/2,485 record 4,992 real time
Mars Orbiter Laser Altimeter (MOLA)	Topography: 50-cm-diameter telescope, 1.06-μm laser, 10 pulses per second, 160-m footprint, and 1.5-m range resolution	25.9	34.2/35.9	618 record
Ultrastable Oscillator (USO/RS)	oscillator provides precision frequency reference for Doppler measurements, especially during exit occultations	1.3	3.0/4.5	N/A
Magnetometer/Electron Reflectometer (MAG/ER)	magnetic fields in the range from 0.004 to 65536 nT; electrons from 1 to 10 keV	5.2	4.6/4.6	324/648/1,296 record
Mars Relay (MR)	Signal relay receiver; interrogating at 437 MHz; receive at 401 and 406 MHz	7.9	9.0/9.05	8,000/128,000 relay rates

most of aerobraking, continuous tracking coverage was provided. In addition, continuous coverage has been provided for special, weeklong science campaigns during mapping to take advantage of special orbit geometry conditions or to observe unique seasonal changes on Mars. In late 1999, as Mars Climate Orbiter and Mars Polar Orbiter approached Mars with their tracking needs, the DSN developed the capability to track several spacecraft simultaneously with a single antenna, significantly enhancing the data return from MGS for that period.

3.4. Propulsion

Propulsion is provided by a dual mode bipropellant system using nitrogen tetroxide and hydrazine. This dual mode differs from conventional bipropellant systems in that the hydrazine is used by both the main engine and the attitude control thrusters, rather than having separate hydrazine tanks for each. The main engine is the only one that used the bipropellant system. The main engine maximum thrust is 659 N. It was used for major maneuvers, including large trajectory corrections prior to entry into the mapping orbit. At launch, MGS carried ~385 Kg of propellant, and nearly 75% of that was used during Mars orbit insertion.

The hydrazine system has four modules, each with three 4.45-N thrusters. Each module contains two aft-facing thrusters and one roll control thruster. The hydrazine system is used for orbit trim maneuvers and unloading the reaction wheels during mapping. These thrusters were also used for keeping the thrust vector in the velocity vector during main engine burns, thereby saving significant propellant on the Mars orbit insertion (MOI) burn.

3.5. Power

Two solar arrays, each 6.0 m^2, provide power for the spacecraft. Each array consists of two panels, an inner and outer panel, composed of gallium arsenide and silicon solar cells, respectively. A combination with the more efficient and more expensive gallium arsenide cells on one of the two panels was utilized because the panels were sized for the aerobraking requirements rather than the power requirements. When the spacecraft moves into eclipse or turns away from the Sun, power is provided by two nickel-hydrogen (NiH_2) batteries, each with a capacity of 20 amp-hours. During cruise the power varied as the solar range increased and with the Sun angle, since the spin axis was normally pointed toward Earth.

During mapping operations an autonomous gimbal drive allows the solar array to track the Sun, acquiring power on the dayside of each orbit. The orbit-averaged power produced by the arrays ranges from 980 W at Mars perihelion to 660 W at aphelion. Eclipses last from 36 to 41 min on each orbit; depth of battery discharge is constrained to be <27%, except during emergencies. The power supply electronics and battery charge assemblies are spare MO hardware.

4. Mars Global Surveyor Science Instruments

The scientific instruments for MGS were designed within the overall architecture of the mission. To meet the scientific objectives of this mapping mission, they had to both acquire high-quality data and maximize the data returned within the constraints of the mission. Each was originally designed and built for the Mars Observer Mission, from which the MGS mission design was derived. However, the mass constraints of the MGS missions made it necessary to restrict the payload to a subset of the MO instruments, leaving two instruments for flight on later missions. All the instruments utilize the design and spare components from the MO mission as well as the same science teams.

MGS carries four onboard science instrument packages and a Radio Science Experiment (Table 2). In addition to instrument principal investigators and the Radio Science Team Leader (hereafter collectively termed PIs), there are a number of Interdisciplinary Scientists associated with MGS (Table 3). Visible imaging and infrared spectral mapping provide information about the nature of the surface and processes operating on the surface. Infrared and radio occultation profiles of the atmosphere provide three-dimensional and time-varying temperature, ice and dust content, and pressure of the atmosphere. The other instruments provide global determination of the topographic, gravitational, and magnetic fields of Mars. MOC, Mars Orbiter Laser Altimeter (MOLA), and TES are coaligned on the nadir platform. These instruments are designed to acquire data along the nadir ground track without moving parts, although TES uses a forward and aft scanning mirror to obtain atmospheric profiles. The instruments have

Table 3. MGS Science Investigations, Lead Investigators, and Interdisciplinary Scientists

Instrument	Lead Investigator	Science Investigation
Mars Orbiter Camera (MOC)	M. Malin, Malin Space Science Systems, San Diego, California	global synoptic view, selected moderate- and high-resolution images of the surface
Thermal Emission Spectrometer (TES)	P. R. Christensen, Arizona State University, Tempe, Arizona	surface mineralogy; atmospheric dust and clouds; radiation budget
Mars Orbiter Laser Altimeter (MOLA)	D. E. Smith, NASA Goddard Space Flight Center, Greenbelt, Maryland	global topography; surface reflectivity at 1.06 μm
Radio Science	G. L. Tyler, Stanford University, Stanford, California	gravitational field; atmospheric refractivity (temperature and pressure) profiles
Magnetometer/Electron Reflectometer (MAG/ER)	M. H. Acuna, NASA Goddard Space Flight Center, Greenbelt, Maryland	global and local magnetic fields and interaction with solar wind
Mars Relay	J. Blamont, Centre National d'Etudes Spatiales, Toulouse, France	relay for planned lander missions

Discipline	Interdisciplinary Scientist	Affiliation
Data Management and Archiving	R. Arvidson	Washington University, St. Louis, Missouri
Geosciences	M. Carr	U.S. Geological Survey, Menlo Park, California
Polar Atmospheric Science	A. Ingersoll	California Institute of Technology, Pasadena, California
Surface-Atmospheric Science	B. Jakosky	University of Colorado, Boulder, Colorado
Climatology	R. Haberle	NASA Ames Research Center, Moffett Field, California
Surface Processes and Geomorphology	L. Soderblom	U.S. Geological Survey, Flagstaff, Arizona

significantly greater computer and data storage capability (Table 2) than those on previous missions, enabling operation continuously during dayside and nightside parts of the orbit, with a single downlink each day. Most have editing and/or compression of their data and can accommodate the differences in downlink capability as the Earth-Mars distance changes.

4.1. Mars Orbiter Camera

MOC is a three-component imaging system (one narrow-angle and two wide-angle cameras) designed to take high spatial resolution images of the surface and lower spatial resolution, synoptic coverage of the surface and atmosphere [*Malin et al.*, 1992; *Malin and Edgett*, this issue]. The cameras are based on the "push broom" technique, acquiring one line of data at a time on a CCD line array as the spacecraft orbits the planet. The cameras share common electronics for storing and processing the data. They are "shuttered" by sending data-processing instructions to the instrument. The instructions are keyed to accurate times, which represent the predicted position of the spacecraft. The narrow-angle camera was designed to sample the surface rather than to acquire images of specific targets. Therefore any targeting of MOC requires sending commands with predicted times (and equivalent positions) well in advance of data acquisition. MOC can output data at a very high rate and can take advantage of any extra real-time downlink capability.

Using the narrow-angle camera at the mapping altitude, areas ranging from 2.8 × 2.8 km to 2.8 × 25.2 km (depending on available internal digital buffer memory) can be imaged at ~1.4 m/pixel. Additionally, lower-resolution images can be acquired by pixel averaging; these images can be much longer, ranging up to 2.8 × 500 km at 11 m/pixel. High-resolution data are being used to study sediments and sedimentary processes, polar processes and deposits, volcanism, aeolian and fluvial erosion and deposition, and other geologic/geomorphic processes. Simultaneous wide-angle images provide positional and meteorological context for the narrow-angle images.

The MOC wide-angle cameras view Mars from horizon to horizon at mapping altitude and are designed for low-resolution global and intermediate-resolution regional studies. The resolution varies from ~250 m/pixel at nadir to ~2 km/pixel at the limb. In a single 24-hour period a complete global mosiac of the planet is assembled from strips taken each orbit at a resolution of at least 7.5 km/pixel. Regional areas (covering hundreds of kilometers on a side) are imaged at a resolution of better than 250 m/pixel at the nadir. These images are particularly useful in studying time-variable features such as lee clouds, the polar cap edge, and wind streaks as well as acquiring stereoscopic coverage of areas of geological interest. To avoid the need for a movable filter wheel, each camera has a single red or blue filter. Images from the two wide-angle cameras are combined to provide color images of the surface and atmosphere that distinguish between clouds and the ground and between clouds of different composition. During the circularization phase of the mission, images were acquired at a variety of Sun angles. In addition, data were acquired covering special targets that were offset from the spacecraft nadir track. This was done by rolling the spacecraft and "shuttering" at predicted times.

More than 75,000 images were acquired prior to the end of the primary mission, more than were acquired by all previous Mars missions.

4.2. Mars Orbiter Laser Altimeter

The primary MOLA objective is to determine globally the topography of Mars by generating high-resolution topographic profiles at a precision suitable for addressing problems in geology and geophysics [*Smith et al.*, this issue (a); *Zuber et al.*, 1992]. The instrument measures the round-trip time of flight of a 1.064-μm laser pulse transmitted from the spacecraft to the surface. Combining these data with accurate location and ve-

locity of the spacecraft allows derivation of surface radii. On some pulses, reflections are also received from ice clouds. The measured reflectivity and nature of the returned laser pulse contribute to analyses of cloud dynamics, seasonal albedo changes, and surface roughness and slope.

MOLA has a diode-pumped, Nd:YAG laser transmitter that emits 8.5-ns pulses at 100-ms intervals with an initial output power of 40 mJ per pulse. The receiving optics, a Cassegrain telescope with a 0.5-m-diameter primary mirror, focuses the return signal on a silicon avalanche photodiode detector. MOLA has a single data rate of 618 bits/s. At the mapping altitude each laser spot illuminates about a 160-m-diameter circle on the surface with a spacing of ~300 m (0.1 sec) per spot along the MGS nadir ground track. The range measurements are quantitized with 1.5-m vertical resolution before correction for orbit and pointing errors. Relative error in altitude along profiles is 1–10 m, and the profiles are being assembled into a global grid referenced to Mars' center of mass with high absolute accuracy.

The demonstration that a laser altimeter can operate for a long lifetime in space is a major accomplishment of this instrument. After firing ~350 billion pulses over a 2-year period, the laser energy had decreased from an initial 45 mJ to 25 mJ on June 1, 2000. MOLA will be operated on alternate months after solar conjunction to conserve laser power for later observations. However, almost 500 million shots were accumulated by the end of the primary mission on February 1, 2001.

4.3. Thermal Emission Spectrometer

TES is designed to study the surface and atmosphere of Mars using thermal infrared spectroscopy, together with broadband thermal and solar reflectance radiometry [*Christensen et al.*, 1992; *Christensen et al.*, this issue]. Objectives include (1) mapping the composition of surface minerals, rocks, and ices; (2) determining the composition, particle size, and spatial and temporal distribution of atmospheric dust; (3) determining the temperature, height, and abundance of water ice and carbon dioxide clouds; (4) studying the growth, retreat, and total energy balance of the polar cap deposits; (5) measuring the thermophysical properties of the Martian surface materials; and (6) characterizing the thermal structure and dynamics of the atmosphere.

TES includes two nadir-pointed telescopes that share a common pointing-mirror system. A 15.24-cm Cassegrain telescope feeds a Michelson interferometer that produces spectra from 1700 to 200 cm^{-1} (~6 to 50 μm), at either 5 or 10 cm^{-1} spectral resolution. The instrument cycle time, including collection of the interferogram, mirror flyback, and electronic reset, is 2 s for 10-cm^{-1} operation and 4 s for 5-cm^{-1} operation. The interferometer includes a visible interferometer that generates fringes which are used to control the linear drive servo and to determine position in the interferogram. This system uses two redundant neon lamps that produce an emission line at 703.2 nm for fringe generation and a continuum that is used for a quasi-white-light source for determination of zero path difference. A digital signal processor is utilized to perform fast Fourier transforms, providing high compression over the raw data. The TES spectrometer has a noise equivalent spectral radiance near 1.2×10^{-8} W cm^{-2} sr^{-1} cm^{-1}. This corresponds to a signal-to-noise ratio (SNR) of 490 at 1000 cm^{-1} (10 μm) viewing a 270-K scene. Calibration is achieved by periodic views of space and an internal reference surface.

A separate 1.5-cm-diameter reflecting telescope, co-collimated with the main telescope and using the same pointing mirror, is used for the bolometric thermal radiance (4.5 to ~100 μm) and solar reflectance (0.3–2.7 μm) channels. A pointing mirror capable of rotating 360° provides views to space, both limbs, and to internal, full-aperture thermal and visible calibration targets, as well as image motion compensation. Each telescope has six detectors, each with a ~8.5-mrad field of view. These form a rectangular grid of three frames in the crosstrack direction and two frames in the downtrack direction. The resulting spatial resolution is about 3 × 2 km at the mapping orbit altitude. The output from TES channels is digitized at 16 bits, processed, compressed, and formatted before being sent to the spacecraft data system. During operation, TES generates data at either 688, 1664, or 4992 bit/s depending upon the phase of the mission. More than 105 million spectra were acquired by the end of the primary mission.

4.4. Magnetometer/Electron Reflectometer

The measurement objectives of the Magnetometer/Electron Reflectometer (MAG/ER) experiment were to determine the existence and characteristics of the global magnetic field, to characterize surface magnetic features, and to determine the nature of the solar wind interaction with Mars [*Acuña et al.*, 1992, this issue; *Mitchell*, this issue]. The experiment includes two redundant triaxial fluxgate magnetometers and an electron reflectometer. The vector magnetometers provide in situ sensing of the ambient magnetic field in the vicinity of the MGS spacecraft over the range of ~1 to 65,536 nT with a digital resolution of 12 bits. The electron reflectometer measures the local electron distribution function in the range of ~1 to 20 KeV and remotely senses the strength of the magnetic field down into the top of the atmosphere using directional information provided by the vector magnetometer. This synergistic combination was designed to increase significantly the sensitivity (factor of 10–100) and spatial resolution (about 3 times) achievable from the mapping orbit with the vector magnetometer alone.

MGS lacks a boom to separate the sensors from the spacecraft body to reduce interference by spacecraft-generated magnetic fields. Instead, each magnetometer sensor is located at the outer edge of the articulated solar panels, ~5 m from the center of the spacecraft bus. This arrangement required a special wiring design and implementation of extremely magnetically "clean" solar array panels. In addition, the spacecraft fields needed to be characterized by calibration maneuvers, both in cruise and in orbit. The electron reflectometer sensor is mounted directly on the spacecraft nadir panel. The instrument acquires 2–16 vector samples per second of magnetic field data, depending on the telemetry rate. Data acquisition, transmission, and command functions are microprocessor controlled and can be partially reprogrammed in flight. About 4.75 billion vector samples were acquired by the end of the primary mission, ~200 million of them during the elliptical orbit period.

The significant advantages of the elliptical aerobraking orbits to the MAG/ER investigation were recognized early in the planning of the observations. In these orbits the spacecraft would dip below the bottom of the Martian ionosphere, allowing the MAG/ER experiment to achieve extraordinary sensitivity and spatial resolution for the detection of weak crustal fields. In addition, the high plasma densities expected at these low altitudes required a different measurement technique, so a

Langmuir probe operational mode was added to the electron spectrometer, using the outer case of the electrostatic analyzer as a swept bias collector [*Mitchell*, this issue].

After only a few orbits it was established that Mars does not now possess a global magnetic field. However, the extended time spent in the elliptical orbit made it possible to characterize remnant crustal fields from pole to pole at a sensitivity and spatial detail that could not have been achieved in the mapping mission as originally planned. Further, the interaction of the remnant magnetic fields with the plasma could be investigated.

4.5. Radio Science Subsystem

Radio science investigations of the gravity field and atmospheric structure have been conducted since the first spacecraft visited Mars, utilizing the telecommunication equipment on the spacecraft in conjunction with the equipment at the DSN stations. Measurements of small perturbations in spacecraft velocity from Doppler shifts on transmitted signals are used to infer detailed gravitational fields from solutions of simultaneous equations using the measurements. During occultation of the spacecraft radio signal by the atmosphere, small Doppler shifts can be interpreted as refractivity changes in the atmosphere; from these, detailed temperature-pressure profiles of the atmosphere can be derived.

The X band capability of MGS reduced solar wind plasma effects on the radio signal by a factor of 10 compared with previous S band systems. In addition, a temperature-controlled Ultrastable Oscillator (USO) was placed on MGS [*Tyler et al.*, 1992, this issue] and was used as a frequency standard during one-way radio science observations, particularly during egress from the eclipse on each orbit. These improvements, combined with the low-altitude polar orbit and dedicated gravity campaigns during favorably geometric configurations for Doppler measurements, have yielded unprecedented spatial resolution, global coverage, and accuracy of the derived gravitational model. Vertical resolution for the atmospheric occultation profiles is close to 10 m, providing an accurate check for infrared measurements, especially during diametric occultation. More than 5000 spectra were acquired during the primary mission.

The Ka band experiment was operated during the cruise to Mars. Measurements showed that the use of Ka band for data transmission could increase data capability by at least a factor of 3 (5 dB) compared to the X band system [*Butman et al.*, 1997].

4.6. Mars Relay

The Mars Relay (MR) system was originally provided to MO and then to MGS by the French Space Agency (CNES) to relay data from the Russian Mars '96 small penetrators and Marskhod Rover to Earth (J. L. Callas et al., manuscript in preparation, 2001). Data was to be routed from MR to the MOC data buffer for storage and subsequent downlink as part of MOC's data return. MR consists of a 1-m helix antenna mounted on the nadir panel and associated electronics, operating at UHF frequencies near 400 MHz. The antenna pattern (−3 dB) forms a 65° cone emanating from the tip of the antenna and provides coverage to the horizon with a 5000-km range for a 8-kbit/s data rate. However, the range drops to ~1300 km for the 128-kbit/s data rate. The system uses a 1.3-W, 437.1-MHz beacon to activate transmission of relay data but essentially provides only a one-way communication link from the surface to the MGS spacecraft.

After the loss of the Mars '96 spacecraft before it left Earth orbit the MR took on a role as the primary communication link for the Mars Surveyor Program Deep Space 2 microprobes and a backup link for the Mars Polar Lander. After the loss of these spacecraft, considerable effort was spent within the MGS mission team in attempting to establish communication with them, but without positive results. Currently, discussions are being held with the Mars '03 mission team relating to using MR to provide a relay link during the landing of those spacecraft.

4.7. Accelerometer and Horizon Sensor

The MGS accelerometer [*Keating et al.*, 1998; *Bougher and Keating*, 1999] and the horizon sensor [*Martin*, 1997] were also used as science instruments during the aerobraking portion of the mission, while assisting in the operation of the spacecraft in the elliptical orbit. They provided information on the density and density changes in the atmosphere in a region where almost no data were available previously. Use of the horizon sensor continues during the mapping mission.

5. Mission Operations and Ground System

5.1. Overview of Distributed Operations

Flight operations for MGS were managed and conducted by the Mars Surveyor Flight Operations Project (MSOP) at the Jet Propulsion Laboratory (JPL), an entity that also became responsible for the simultaneous operation of Mars Climate Orbiter and Mars Polar Lander. Surveyor flight operations are characterized by remote (from JPL) control of the science instruments and spacecraft. The science investigation teams are located at the home institutions of the Principal Investigators (PIs), Team Leader, and Interdisciplinary Scientists. The spacecraft operations are conducted by Lockheed Martin Astronautics at its Denver, Colorado, facility, where the spacecraft was built and tested. The MGS project performs mission management, navigation, data administration, and mission planning and sequence development at JPL. Workstations and electronic communication links connect the mission planning and data analysis activities of the scientists and engineers with JPL, where tracking data are received from the DSN and stored and where command messages for the spacecraft are assembled.

The MGS mission utilizes data standards for packet telemetry and telemetry channel coding and a standard formatted data unit for data transfer among ground systems. Mission data are stored in a central Project Database at JPL. Raw science data consist of science and engineering packetized telemetry data, together with spacecraft position and pointing information data available as a supplementary experiment data record. Planning products include the up-to-date mission sequence plan, schedules and commanding opportunities, and orbit/viewing forecasts. Investigators and analysts access the Project Database to participate in the planning process and to acquire raw data.

The DSN acquires and handles science and engineering telemetry from the spacecraft, as well as radiometric data to support navigation and radio science objectives. Multimission capabilities at JPL were used for telemetry processing, flight system commanding, data system operational control, and telecommunications link performance assessment. The telemetry processing includes error detection and correction using the Reed-Solomon encoding information supplied with the data from the spacecraft, depacketization of the transfer frames, placement of the packets into the Project Database for access

by the investigators, transfer of the engineering data for display at the analysis's workstation, and monitoring of spacecraft engineering data for assessing the health of the spacecraft. The project also provides spacecraft performance analysis, spacecraft navigation, and flight system command sequencing.

5.2. Science Operations Planning Computer

A Science Operations Planning Computer (SOPC) is located at the home institution of each Team Leader, Principal Investigator, and Interdisciplinary Scientist. Each SOPC has restricted access and is connected to the Project Database via NASA Communications (NASCOM) circuits. The SOPCs enable the instrument teams to exercise substantial direct control of their instruments and enable the interdisciplinary scientists to be directly involved in mission operations. Command sequence software is resident on each SOPC, enabling the investigators to prepare nearly all of the commands required by their instruments to conduct the desired experiments and to forward those commands directly to the command request file in the Project Database.

5.3. SPICE System

SPICE is an acronym used to describe five basic kernels of data needed to provide critical information for processing science data files: S stands for spacecraft ephemeris, spacecraft location as a function of time; P stands for planetary ephemerides and selected physical and cartographic constants; I stands for instrument descriptions, including identification codes used in E kernels and alignment offset angles used in C kernel; C stands for inertial orientation of the spacecraft primary coordinate system in right ascension, declination, and twist angles and rate changes for the coordinate system; and E stands for event information, including nominal sequences, real-time commands, unscheduled events, and experimenter's notebook comments [*Acton*, 1991]. Ancillary data are packaged as SPICE kernels and made available for processing data.

The kernels are used together with a software tool kit supplied by the Navigation and Ancillary Information Facility (NAIF) at JPL to calculate the basic information required by the investigators in analysis of the experiment data records. SPICE kernels are generated by various mission operations teams on the basis of orbital tracking, together with instrument information and sequence data obtained from instrument teams. MGS uses both "actual" and "predict" SPICE files. Predict SPICE kernels are generated in advance as part of the sequence planning cycle. This capability is especially useful for predicting when an instrument will have an opportunity to observe a feature of interest. The actual SPICE kernels are generated within several weeks after data acquisition for use during the science analysis by each of the experiment teams. The SPICE data sets and the associated software tool kit are released regularly and archived for use with the archived science data.

5.4. Commanding-Uplink Process

The primary command processing consists of generating periodic (typically 1 week) Stored Sequence Command loads that control spacecraft bus operations and update onboard spacecraft ephemerides and star catalogs. Each new load is generated by an adaptive process, modifying skeleton sequences built and tested previously. However, since instrument operation is nearly independent of spacecraft operations, each PI may request transmission of noninteractive real-time commands to their instrument at any time. DSN coverage is scheduled in advance. Using the skeleton sequence for each multisol cycle, the science investigators develop their observation plans, produce a set of files using sequence software provided with their SOPC, and transmit them to the Project Database as sequence requests via the SOPC. Most requests are updates to tables in the memory of the individual instrument. Interactive real-time commands are, by definition, those that affect another instrument or spacecraft subsystem. They are tagged as such and subjected to validation in the command process. The use of these interactive commands is not common. Mission operations personnel at JPL complete the command process by integrating the independently developed sequence requests, verifying that no spacecraft or mission constraints are violated, and translating the sequence into a command file for uplink to the spacecraft by the DSN.

5.5. Data Return-Downlink Process

The MGS downlink process consists of a daily playback of the spacecraft solid state recorders plus a real-time data return about every third day. The science data are placed in the Project Database in packets as formatted by the instrument. Averaged over the mission, the raw data rate is more than 120 Mb/d. The SOPCs provide the instrument teams with access to the science telemetry packets within 24 hours of their receipt by the DSN and the SFOC. The science teams are responsible for generating quick-look science data and/or examining housekeeping data to monitor instrument performance on the basis of the data in the experiment data packet.

6. Science Data Management and Archiving

Any one instrument on MGS produces a large volume of data that when analyzed, will significantly augment our understanding of Mars. In addition, cross-instrument analyses allow questions to be addressed that are difficult or impossible to answer with information from a single instrument. Because of the scientific importance of the new data from MGS and the widespread public interest in new results from Mars, formal data sharing and release policies have been established. Further, each experiment team has committed to the generation and timely release of archives of MGS-derived products to NASA's Planetary Data System for distribution to the research, education, and public communities.

6.1. Data Use Policy

The data rights policy lays out broad guidelines on the use and release of data to ensure that the science done with MGS data is maximized and that the expertise of MGS scientists is utilized in the best possible ways. The PIs have primary responsibility for the acquisition, reduction, analysis, and production of archival data sets for the data obtained from their instruments. They are also responsible for publishing scientific results and for timely deposition of reduced data and documentation with the project. All MGS scientists are encouraged to participate actively in collaborative efforts. The authorship of collaborative publications has generally included all participants in the reduction and analysis of data.

6.2. Data Release and Archiving

A cornerstone of the MGS data release policy is that the release of data to the Planetary Data System archive depends only on the amount of time required to accumulate sufficient

Table 4. Mars Global Surveyor Standard Data Products

Instrument	Archive Internet Access	Description
Accelerometer	http://atmos.nmsu.edu/mgsacc.html	accelerometer counts, periapsis orbital elements, angular rates and quaternions, thruster-on times, density profiles, constant altitude profiles
MAG/ER	http://www.igpp.ucla.edu/ssc/pdsppi/mgsmag.htm	magnetometer magnetic field vectors, Electron Reflectometer omnidirectional flux
MOC	http://ida.wr.usgs.gov/	narrow-angle and wide-angle images
MOLA	http://wufs.wustl.edu/missions/mgs/mola/	raw and precision orbit corrected altimetry profiles, gridded global topography maps
Radio Science	http://pds-geophys.wustl.edu/pds/mgs/rs/	occultation summary file; atmospheric temperature-pressure profiles; surface reflection images, tables, and geometry; ionospheric electron density profiles; intensity power spectra; line-of-sight acceleration profiles; spherical harmonic models of gravity field; Radio Science digital maps
SPICE	http://wufs.wustl.edu/missions/mgs/spice.html	spacecraft and planet ephemeris; Mars size, shape, and orientation (nominal pre-flight values); instrument mounting alignments and field-of-view specifications; orientation of spacecraft, solar arrays, and high-gain antenna; high-gain antenna reference frames specifications; spacecraft clock coefficients; leapseconds tabulation
TES	http://wufs.wustl.edu/missions/mgs/tes/	observational parameters; raw and calibrated radiance observations; raw and calibrated visual and thermal bolometer measurements; Sun, spacecraft, and planet geometric data; positional information for spacecraft, Sun, and Mars; auxiliary observation parameters; raw interferogram data; real and complex FFT data; derived surface properties; derived parameters from planetary limb observations; global derived surface property maps

data and information to generate standard products, to conduct the work needed to generate the products, and to check the validity of the results. The default period for this activity spans a nominal 6-month period from the receipt of raw data at the home institution responsible for generating the relevant standard data product to release of documented archives containing the products to the PDS. During this period the Instrument Teams produce and validate standard data products, submit for publication their preliminary analysis, and work with the PDS to assemble archive volumes and Web-based ftp sites for release to the community. Table 4 lists the standard products and the Web access and Figure 5 is a summary of the number and volume of data products released to the Planetary Data System as a function of time.

7. Mission Phases and Events

The MGS spacecraft was launched on November 7, 1996 (Figure 2). The spacecraft maintained a slow controlled roll in a partially deployed state during its 11-month flight to Mars. After orbital insertion into a 45-hour elliptical orbit on September 11, 1997, MGS utilized repeated dips into the upper atmosphere to aerobrake and attain the low index altitude (378-km) circular-mapping orbit. MGS should have reached this orbit early in spring of 1998. However, failure of a solar panel damper during deployment immediately after launch resulted in damage to a panel, the extent of which did not become clear until about a month into aerobraking. At that time, periapsis altitude was raised to 174-km altitude to lower atmospheric pressure on the panel while the problem was under assessment. Excellent, although unanticipated, science data were acquired during this 1-month period as alternative plans were considered. The revised mission plan preserved the mission architecture but delayed entry into the circular-

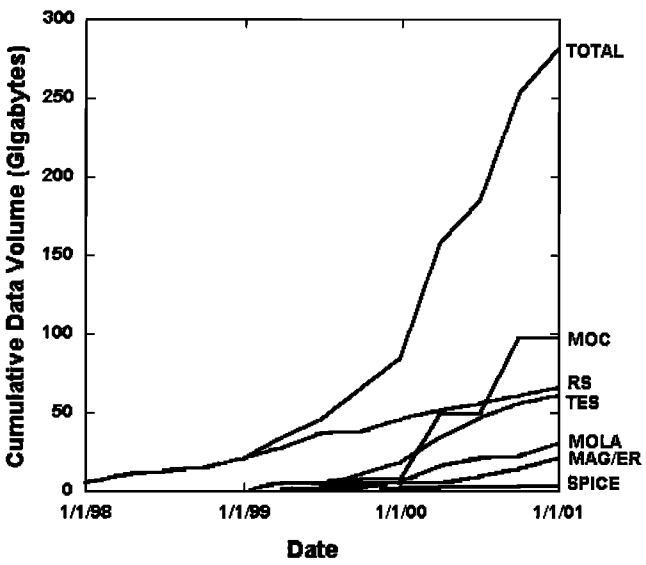

Figure 5. MGS data volume over time by individual experiments.

mapping orbit for an entire Earth year, requiring a long phasing period in elliptical orbit and many more-modest aerobraking passes into the atmosphere. The spacecraft reached the 378 km circular orbit on February 19, 1999, but in the 0200 LT (relative to the Sun) position rather than in the originally planned 1400 LT position.

7.1. Launch, Cruise, and Orbit Insertion

The MGS spacecraft was launched from Cape Canaveral Air Force Station, Florida, on November 7, 1996, aboard a McDonnell Douglas Delta II 7925 rocket, a configuration with nine strap-on rocket motors. Weather conditions delayed the launch until the second day of the launch window. The 1062-kg spacecraft, built by Lockheed Martin Astronautics, traveled nearly 750 million km over the course of a 300-day cruise to reach Mars on September 11, 1997. Deployment of the solar arrays and checkout of the spacecraft and instrument systems was carried out early in cruise using the low-gain antenna. After 4 months, communications were shifted to the high-gain antenna, still in its fixed position on the spacecraft. After deployment of the solar array panels it became clear that one of them was not locked in its proper position. After a series of flexing experiments it was decided to reverse the orientation of that panel for the entry into Mars atmosphere.

Upon reaching Mars, MGS was inserted into orbit by firing the main bipropellant rocket engine for a 23-min Mars orbit insertion (MOI) burn. A "pitchover" maneuver, keeping the thrust vector parallel to the velocity vector, saved ~20 m/s in propellant [*Esposito et al.*, 1998]. The initial MGS orbit was highly elliptical with a period of 44.993 hours, a periapsis altitude of 262.9 km, an inclination of 93.258°, and an orientation of ~1800 LT relative to the sunline.

7.2. Circularization

During the third periapsis at Mars the spacecraft was pointed to the nadir to enable the instruments to operate and collect data in order to verify that they were working properly. On the third orbit, MGS initiated the aerobraking period, utilizing repeated dips into the upper atmosphere with the solar panels in a V configuration to slow it so as to attain the low-altitude (378-km) circular-mapping orbit. Aerobraking was a key feature of the MGS mission, required because the injection capability of the Delta II is not sufficient to launch the mass of fuel required to use chemical propulsion to establish the mapping orbit. According to plan the spacecraft would have reached the mapping orbit in the spring of 1998, before the solar conjunction period (see Figure 6 and Table 5).

However, at the low point of orbit 15 on October 8, 1997, the spacecraft experienced excessive flexing of one of the solar panels. The damper failure during solar panel deployment in early cruise resulted in damage to the yoke of the panel, the extent of which did not become evident until the spacecraft dipped far into the atmosphere. The orbit was quickly raised higher in the atmosphere to lower the pressure on the panel. In orbits 19–36 (October 13, 1997, to November 7, 1997) the periapsis altitude was only 175 km, and the spacecraft passed in and out of the ionosphere on each orbit. The science instruments were operated in the nadir orientation in the near-periapsis portion of each 35.4-hour elliptical orbit, collecting data as the spacecraft moved from north to south. The first extensive sets of scientific observations were collected from this assessment or hiatus period during the hiatus from aerobraking as alternative plans were considered [*Albee et al.*, 1998].

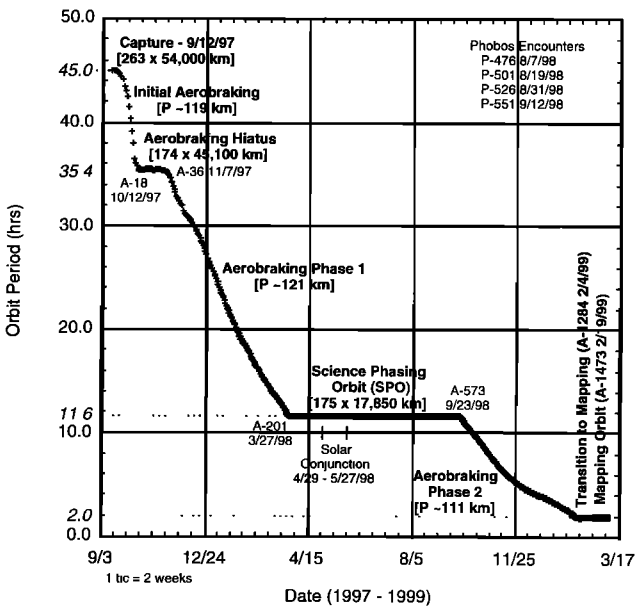

Figure 6. MGS aerobraking phase: orbit period and size versus date. The location of periapsis migrated from 45° north over the north pole and then down and over the south pole.

After considerable analysis, aerobraking was resumed on November 7, 1997, with reduced pressure on the panels. The original plan was to reach the mapping orbit prior to the period of solar (superior) conjunction. The revised mission plan delayed the entry into the circular-mapping orbit for an entire Earth year, requiring many more aerobraking dips into the atmosphere, but with only one third as much pressure being exerted on the solar panels. The dynamic pressure was reduced from the planned 0.68–0.58 N/m^2 corridor to 0.25–0.15 N/m^2. The spacecraft finally reached its final 378-km near-circular orbit on February 19, 1999, but in the 0200 LT (relative to the Sun) position rather than in the originally planned 1400 LT position. This delay of half a Mars year was undertaken since it made it possible to operate the spacecraft and its instruments in the geometric relationships for which they had been designed. However, the spacecraft would ascend from south to north on the daylight side of the orbit in this position (Figure 1).

Scientific observations were obtained during most of the year period of delay. Low-altitude (high-resolution) data, especially important for the magnetometer and gravity investigations, were obtained with coverage over most of the planet. Such coverage was possible because during this period of time the periapsis position of the continuously decreasing elliptical orbit migrated from 45° north over the north pole and then down and over the south pole. Correct phasing of the entry into a 1400 LT circular orbit necessitated a substantial pause (SPO-1 and SPO-2) in the aerobraking operation, during which science data was collected from 372 elliptical orbits, 175 × 17,800 km, from March 27, 1998, to September 23, 1998. During the periapsis-passage portion of each 11.6-hour orbit the spacecraft was turned to the nadir-pointing position so that the instruments pointed to Mars for ~22 min. MOLA, TES, and MOC obtained data in near-normal mode during the nadir portion of these orbits and acquired lower-resolution global

Table 5. MGS Events Subsequent to Mars Orbit Insertion[a]

Events[a]	Orbit[b]	Periapsis Date	Orbit Period,[c] hours	Periapsis Altitude,[c] km	Apoapsis Altitude, km	delta V, m/s
Mars orbit insertion burn (MOI)	P-1	Sept. 12, 1997	44.993	262.9	54,026	973
Orbit nadir-pointed at periapsis	P-2					
Apoapsis burn	P-3	Sept. 15, 1997	45.3	263	54,026	4.4
Aerobraking period: initial						
Apoapsis burn	P-18	Oct. 12, 1997		~115		
Hiatus/assessment period	P-19	Oct. 13, 1997	35.4	175	45,100	
(nadir-pointed at periapsis)						
Apoapsis burn	P-36	Nov. 7, 1997	35.4	175	45,100	
Aerobraking period (AB-1)						
Apoapsis burn	P-201	March 27, 1998		~125		4.4
Science phasing orbits (SPO1)	P-202	March 27, 1998	11.6	175	17,800	
(nadir-pointed at periapsis)						
Solar conjunction period	P-269	April 29, 1998				
Science phasing orbits (SPO2)	P-328	May 27, 1998				
Phobos encounter	P-476	Aug. 7, 1998				
Phobos encounter	P-501	Aug. 19, 1998				
Phobos encounter	P-526	Aug. 31, 1998				
Phobos encounter	P-551	Sept. 12, 1998				
Apoapsis burn	P-573	Sept. 24, 1998	11.6	175	17,800	11.6
Aerobraking period (AB-2)				~127		
End of walkout				143	450	
Apoapsis burn (ABX)	P-1284	Feb. 4, 1999				61
Gravity/MOC calibration	P-1285	Feb. 4, 1999	118 min	377	454	
Adjustment burn (TMO)	P-1473	Feb. 19, 1999				22
Final partial orbit	P-1683	March 9, 1999				
Mapping orbits (MO)	DEX-1	March 9, 1999	118 min	367.8	438.5	
Deploy HGS/go to nadir point	DEX-247	March 29, 1999				
Mapping configuration	DEX-1000	May 29, 1999				
Beta supplement configuration	DEX-4110	Feb. 7, 2000				
	DEX-5000	April 20, 2000				
End of nominal mission	DEX-8506	Feb. 1, 2000				

[a]Mission phases may be referred to as AB-1, AB-2, SPO-1, SPO-2, and MO.
[b]Premapping orbits are labeled P-1 to P-1683, beginning with the periapsis of the MOI orbit. Mapping orbits are labeled DEX for Descending Equatorial Crossing.
[c]During each of the three aerobraking periods the orbit period and the apoapsis altitude decrease continuously from the upper values to the lower values.

image and thermal data during the rollout from the nadir position to the Earth-point position. MAG/ER obtained data throughout the entire orbit during most of this period. Because the HGA was not deployed, radio tracking was limited to the higher portions of the orbit, where the spacecraft could point the HGA toward Earth.

Science data were also obtained during the aerobraking phases (AB-1 and AB-2), both before and after the two periods of science-phasing orbits (Figure 6). Although science data acquisition during the aerobraking phase was not in the original mission plan, MOC, TES, ER, and the spacecraft's accelerometer and horizon sensor all acquired data, which were used to predict atmospheric density on subsequent orbits. During the aerobraking passage through the atmosphere the spacecraft had the solar panels in a V configuration with the instrument panel in the lee direction. The accelerometer data provided density profiles of this atmospheric passage. At the close of aerobraking as the spacecraft exited the atmosphere it rolled to point the HGA back toward Earth. During these rollouts, MOC and TES obtained visual and thermal coverage over much of Mars. MAG/ER data were acquired throughout each orbit. Gravity measurements and atmosphere profiles were obtained from radio tracking of the orbit, and accelerometer measurements were obtained during the aerobraking portion of the orbits. MGS returned 2140 MOC images, 11 million TES spectra, 206 MOLA profiles with 2.6 million points, 465 radio-occultation profiles, and 1000 MAG low-altitude passes during this unexpected bonus period of observation prior to the primary mission. Moreover, atmospheric data were obtained over a range of daily times, other than the fixed 0200/1400 LT position of the mapping mission. In addition, data were acquired during three close encounters with Phobos.

Periods of data acquisition may be referred to as the hiatus period and the aerobraking periods (AB-1 and AB-2), separated by the science-phasing periods (SP-1 and SP-2, separated by solar conjunction).

It was known from earlier missions that the atmospheric density of Mars at the aerobraking altitude would show great variation over time as well as large orbit-to-orbit differences and that major dust storms are most likely to develop at the time of year at which aerobraking was to be initiated. So that the spacecraft could adjust its orbit, the density had to be predicted for each orbit in order to adjust the spacecraft trajectory to an appropriate and safe depth within the atmosphere for the next aerobraking passage. More important, it was necessary to avoid any high-pressure excursions that could damage the weakened solar panel and cause loss of the spacecraft. Doppler tracking of the spacecraft and accelerometer measures provided the key measurements of the atmospheric density. In addition, the science instruments on the spacecraft as well as images from Hubble Space Telescope and ground-

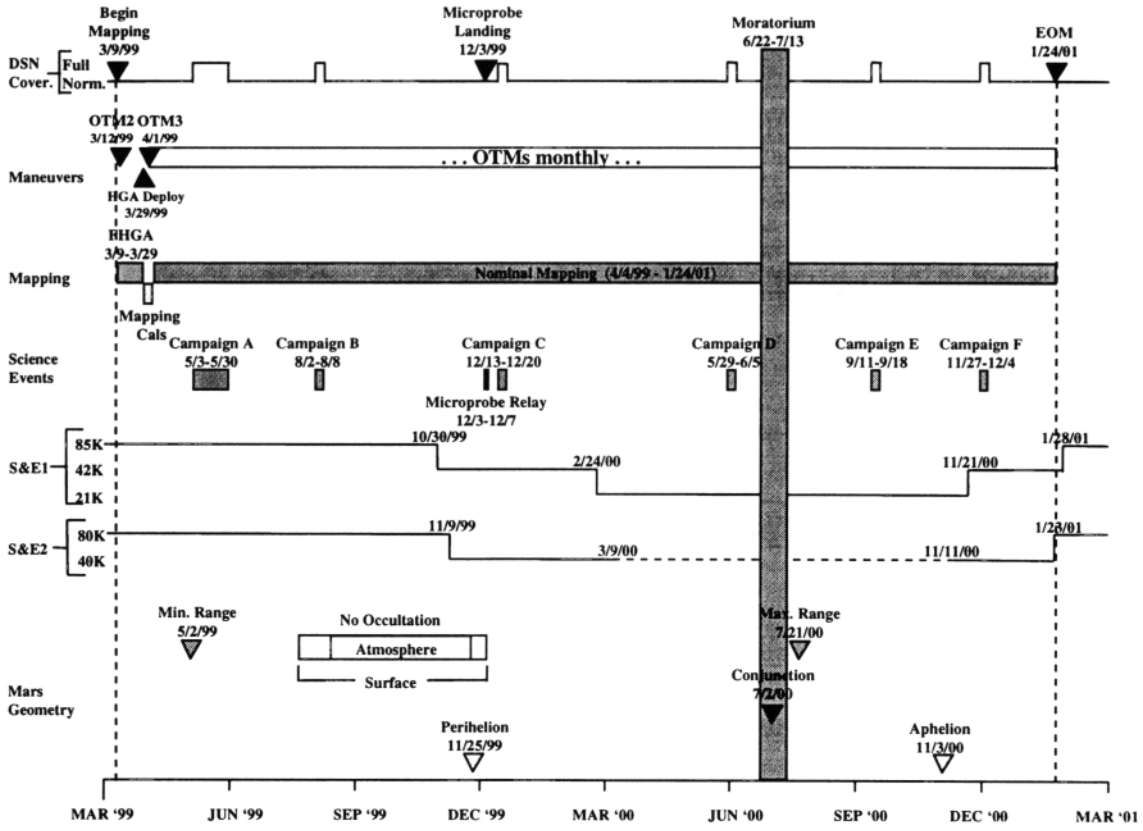

Figure 7. Timeline for MGS mapping period showing science campaigns, changes in data rate, and planned support for the Mars microprobe and Mars Polar Lander. Note that the formal end of mission will be January 31, 2001 (Pacific Standard Time).

based whole-disk microwave observations were utilized to provide advance warning of dust storms that could trigger density excursions at the aerobraking altitude. Plotting of density data against longitude displayed an unexpected periodicity with peaks near 90° and 270° east longitude, and this dependency was utilized to provide more accurate estimates of atmospheric density [*Esposito et al.*, 1998; *Keating et al.*, 1998].

During AB-2 the orbit period became shorter, and corrections were not made on every orbit. During the final period of aerobraking as the apoapsis reached 450 km the spacecraft was "walked out" of the atmosphere by gradually raising its periapsis to 143 km. A 2-day orbit lifetime constraint was maintained by making four small burns so that if a spacecraft anomaly occurred, there would be sufficient time to recover and perform a raise maneuver to maintain planetary protection provisions. Aerobraking ended with a termination burn (ABX) on February 4, 1999, when the descending node had reached a 0204 LT orientation, placing MGS in a 377 × 454 km orbit (Table 5). At this point the periapsis latitude was ~60° south, while continuing to drift ~3° per day southward. On February 19, 1999, a transfer to mapping burn (TMO) was executed to place the spacecraft in the mapping orbit with periapsis passage locked over the south pole. Continuous radio tracking was carried out between the two burns in order to provide a new and much more accurate gravity field for Mars for use during subsequent mapping operations.

The geometry for data acquisition during this period changed continuously. To indicate this, data may be described as having been acquired during hiatus (or assessment) orbits, during aerobraking orbits (AB-1 or AB-2), broken by the science-phasing orbits (SPO-1 or SPO-2), and broken in turn by solar conjunction orbits (Table 5 and Figure 6), during which no data were returned.

After more than 17 months in orbit, MGS reached its mapping orbit on February 19, 1999. For the first time a spacecraft had successfully deployed aerobraking techniques to reach its desired mapping orbit at Mars. Figure 7 and Table 6 show that the orbit period had been reduced from 45 hours to 2 hours during 299 days of aerobraking, which saved ~1250 m/s of propellant. The MGS spacecraft (and the operations teams) performed 891 drag passes, executed 92 trajectory control maneuvers, survived the onset of a Martian dust storm that tripled dynamic pressure values at aerobraking altitudes, and avoided collision with Phobos during four close encounters [*Esposito et al.*, 1999; *Johnston et al.*, 1999].

7.3. Mapping

The MGS mapping mission was initiated on March 9, 1999, after a period of final orbit adjustment, spacecraft checkout, and instrument calibration (Figure 7). A problem was anticipated with the strength of the damper used to control the deployment rate of the HGA boom, since it was similar to the one that failed on the solar panel. As a contingency, one global data set was acquired over a 3-week period with the HGA in the stowed position. The spacecraft alternated between two orientations: the standard nadir-mapping configuration for nine orbits per day and one with the fixed HGA pointing toward Earth for data transmission for three orbits per day.

Table 6. Science Campaigns and Important Geometric Events Subsequent to Mars Orbit Insertion

Date	L_S	Event	Comments
April 24, 1999		opposition	Sun-Earth-Mars angle at 178.62°
May 3–30, 1999	135°	science campaign	northern midsummer/southern spring
May 2, 1999		Mars to Earth range at minimum	0.578 AU distance
July 21, 1999		begin no surface occultation	Earth beta angle at 64.4°
Aug. 1, 1999		autumn equinox	start of southern spring
Aug. 2–8, 1999	181°	science campaign	start of southern spring/northern fall
Aug. 13, 1999		begin no atmosphere occultation	Earth beta angle at 68.1°
Aug. 18, 1999		solar beta angle at maximum	beta angle at 39.61°, solar eclipse of 35.5 mins
Oct. 6, 1999		Earth beta angle at maximum	Earth beta angle at 75.49°
Oct. 16, 1999		southern declination at maximum	Mars declination at −25.21 as seen from Earth
Nov. 24, 1999		end of no atmosphere occultations	Earth beta angle at 66.7°
Nov. 25, 1999		perihelion	solar distance at 1.381 AU
Dec. 6, 1999		end of no surface occultations	Earth beta angle at 62.9°
Dec. 13–20, 1999	261°	science campaign	start of southern summer/northern winter
Dec. 25, 1999		winter solstice	start of southern summer
April 1, 2000		solar beta angle at minimum	beta angle at 16.80°, solar eclipse of 40.5 min
May 29–June 5, 2000	359°	science campaign	start of northern spring/southern fall
June 18, 2000		northern declination at maximum	Mars declination at −24.22°, as seen from Earth
June 22, 2000		begin command moratorium	start solar conjunction period, Sun-Earth-Mars angle <2°
July 2, 2000		solar conjunction	Sun-Earth-Mars angle reaches a minimum of 0.56°
July 13, 2000		end command moratorium	end solar conjunction period, Sun-Earth-Mars angle >2°
July 21, 2000		Mars to Earth range at maximum	distance of 2.621 AU
Sept. 11–18, 2000	45°	science campaign	northern midspring/southern fall
Nov. 3, 2000		aphelion	solar distance at 1.666 AU
Nov. 27–Dec. 4, 2000	81°	science campaign	late northern spring/southern fall
Dec. 15, 2000		diametric occultation	Earth beta angle at 0.0°, Earth occultation of 41.3 min
Jan. 24, 2001		Earth beta angle at extended minimum	Earth beta angle at −1.5°

The HGA was finally deployed on March 29, 1999, and continuous nadir pointing operations were initiated, requiring the HGA to track Earth and return data at the same time that the instruments were acquiring data.

Unfortunately, the full motion of the HGA azimuth gimbal was and is still limited by an obstruction of some kind. The limitation on the motion did not restrict simultaneous Earth tracking and data acquisition until February 2000. It proved possible to work around this problem by driving the gimbal from the opposite direction, the Beta Supplement mode. However, radio occultation measurements in both hemispheres are not possible in this mode over an extended time period (February 7, 2000, to April 22, 2001). During this period it remains necessary to periodically point the HGA toward Earth to acquire such data.

The mapping orbit has a nodal period of 117.65 min, an 88-revolution near-repeat cycle lasting ~7 sols (Martian days), and an index altitude of 378 km (Table 1). Figure 7 provides a timeline for the mapping phase of the mission and Table 6 lists the important geometric events during the same period. In the nominal mapping mode the spacecraft is continuously nadir-pointed, enabling the instruments to acquire and record data on a continuous basis. Daily, the recorded science and engineering data (S&E 1) are transmitted back to Earth during a single 10-hour tracking pass using a 34-m DSN station. In addition, real-time data (S&E 2) may be collected and transmitted at a high rate during additional tracking passes scheduled about every third day. Three S&E 1 rates and two S&E 2 rates are used at various times during the mission since the useful telemetry data rate varies substantially with distance from Mars to Earth (Figure 7). Telemetry is interrupted for a period around solar occultation. The scientific return has been significantly enhanced by the use of the science campaigns shown on the timeline (Figure 7). Continuous 24 h/d tracking has been utilized during these periods of special geometrical or seasonal interest. Campaign A was termed the Geodesy Campaign and had the objective of obtaining global stereo and color coverage early in the mission [*Caplinger and Malin*, this issue].

Additional real-time downlink became available in the fall of 1999 as the Mars Climate Orbiter and the Mars Polar Lander spacecraft approached Mars. This was a result of technical developments that enabled the DSN to simultaneously track and receive data from more than one spacecraft with a single antenna station. Much of this additional downlink was devoted to acquiring additional characterization of the Mars Polar Lander landing site. MGS also had the responsibility of using its onboard radio relay antenna to relay data from the microprobes and the lander and, after their loss, continued attempts to establish communications with the landed spacecraft.

The nominal mapping mission will end on February 1, 2001 (January 31 at 1643 LT) at the start of orbit 8506 (Table 6). The planned 3-year relay period following the mapping period was established to use the spacecraft's Mars Relay system to provide a Mars to Earth relay function for future lander missions of the United States or of other nations. During this period a maneuver would raise the orbit to a near-circular orbit of 400 km or more to assure that the probability for the unsterilized spacecraft impacting the planet meets the international requirements for planetary protection. However, the additional knowledge of the atmosphere from MGS may remove the need for a raise maneuver and allow an extension of the mapping mission. Potentially, the mapping period could be extended to about August 2004, more than doubling the number of mapping orbits over that achievable in the prime mapping mission. In addition, MGS could serve as a relay orbiter for the 2003 lander missions.

8. Overview of Scientific Results

Most of the science objectives require mapping that results in derived data sets that have spatial and temporal dimensions. For the geoscience objectives, products are generated that depict surface and subsurface characteristics as a function of latitude, longitude, elevation, and season. For many climatology objectives the data sets are organized by latitude, longitude, altitude, and season. MGS has already obtained a systematic global characterization of Mars as it exists today. This characterization, supplemented by the data from the remainder of the mission, will dramatically increase our understanding of the geologic and climatologic history of Mars and the evolution of its interior and surface and will provide databases for comparison with Venus and Earth.

8.1. Geoscience

Mars is a single-plate planet, with a surface area that is slightly larger than the combined area of all the plates that make up Earth's continents, ~144 million square kilometers. The systematic measurements made by MOC, MOLA, TES, MAG/ER, and RS have dramatically increased our understanding of the geology and geophysics of the Red Planet. In the subsections below we summarize some key results obtained by the end of the first year of mapping.

8.1.1. The Martian crust and interior. The most distinctive and enigmatic feature on the surface of Mars has been the hemispheric dichotomy between the old, highly cratered southern highlands (i.e., Noachian age crust) and the younger, sparsely cratered northern plains. MOLA data have been used to produce a very high fidelity map of the shape and topography of Mars [*Smith et al.*, this issue (b)]. The global topography of Mars is now known to greater accuracy than Earth's continents in a root mean square sense [*Smith et al.*, 1999a]. The ellipsoidal shape is flattened by ~20 km owing to rotation, and the center of figure is offset from the center of mass by 2986 m along the polar axis, indicating that the north pole is ~6 km lower than the south pole. As pointed out by *Bills and Ferrari* [1978], this offset requires that the density distribution for Mars is not radially symmetric and is consistent with a thicker crust in the southern highlands. In addition, the center of figure is offset from the center of mass ~1428 m toward the Tharsis topographic rise.

The topography of Mars has a range of 30 km from the lowest point in Hellas to the top of Olympus Mons. This range is the largest for any terrestrial planet and much larger than the 20 km range of Earth. MOLA data also show that the northern lowlands are exceeding smooth and level, and if Mars had running water, water would collect in these areas after draining from the southern highlands. The Hellas impact basin has a total relief of more than 9 km. The main basin with a diameter of ~2300 km is surrounded by a highly cratered annulus lying ~2 km above the edge of the main basin. Material thrown out from Hellas accounts for a significant contribution to the higher topography of the southern hemisphere.

The hemispheric dichotomy marks both a difference in elevation and a difference in geologic setting. Various hypotheses to explain these differences have included (1) thinning of the northern hemisphere crust by mantle convection, (2) an early period of tectonic plate recycling, and (3) large impacts in the northern hemisphere. The MOLA data demonstrate that the offset between the center of figure and the center of mass accounts for much of the elevation difference between the two hemispheres; it further suggests that the hemispheric elevation difference is primarily a long-wavelength effect due to large-scale differences in the crustal thickness. It has been suggested [e.g., *Smith et al.*, 1999b] that the dichotomy boundary, as manifested in surface geology and regional topography, appears to contain three dominant contributions: (1) volcanic constructions associated with Tharsis, (2) major excavated deposits approximately circumferential to Hellas, with additional contributions from Isidis and probably Utopia ejecta, and (3) modification of the intervening region by fluvial processes associated with the outflow channels that empty into Chryse Planitia.

Knowledge of both the gravity field from RS and the surface topography from MOLA at similar scales is key to understanding the internal structure of the planet. Removal of the gravitational signal due to the mass of the topography makes it possible to gain some understanding of the internal density anomalies that are associated with thermal or compositional differences. MGS observations of the gravity field of Mars [*Tyler et al.*, this issue] show that the anomalies correlate well with the principal features of the topography, including volcanic constructs, impact basins, and Valles Marineris. However, the planet has responded differently in its northern and southern hemispheres to major impacts and volcanic processes. The rough, elevated southern hemisphere has a relatively smooth gravitational signature, indicating a state of near-isostatic compensation, whereas the low, flat northern plains display a wider range of uncompensated gravity anomalies that indicates a thinner but stronger crustal layer than in the south. To first order, the 6-km difference in elevation from pole to pole can be accommodated by a 30-km thinning of the crust from the south pole to the north pole. In general, the dichotomy boundary does not have a distinct gravitational signature. Mascons, gravity highs associated with topographic lows, are present in the Argyre, Hellas, and Isidis basins. The northern hemisphere shows evidence for buried impact basins, though none are large enough to explain the hemispheric elevation difference. The gravitational potential pattern of Tharsis is approximately axisymmetric and contains the Tharsis volcanoes, but the Olympus Mons and Alba Patera volcanoes seem to be adjacent, separate features. The gravity signature of Valles Marineris extends into Chryse Planitia and provides an estimate of material removed by early fluvial activity.

MAG/ER observations during the circularization phase of the mission conclusively showed that Mars now lacks a global internal magnetic field [*Acuña et al.*, 1998]. This result resolved a long-standing controversy and places an important constraint on the present nature of the Martian core. More important, however, MAG/ER observations showed crustal magnetic anomalies of surprisingly high strength in the older rocks of the southern hemisphere [*Acuña et al.*, 1999]. These anomalies demonstrate that Mars had an early internal dynamo. The lack of such high magnetic strength in the northern lowlands and the major volcanic constructs associated with Tharsis implies that the internal dynamo had ceased to operate by this time of formation of these structures.

MAG/ER mapped parallel bands, ~200 × 1000–2000 km, in the southern highlands that show reversals in the radial magnetic field direction from inward pointing to outward pointing in adjacent bands [*Connerney et al.*, 1999]. Some show a magnetic moment an order of magnitude greater than any known on Earth. The linear pattern, the reversal in polarity, and the size of the magnetic moment each present problems in inter-

pretation that are not yet resolved. On Earth, linear magnetic patterns of alternating polarity are associated with seafloor spreading and repeated reversals of the global dipole field of Earth. Molten magma is injected from below, cools below its Curie temperature, and acquires a permanent remanent magnetic moment aligned with the terrestrial dipole field. The typical spreading rate and the typical reversal period lead to a characteristic width of ~10 km for such features. By comparison, Mars would require a faster spreading rate or a longer period between magnetic reversals. The magnitude of the magnetic moment introduces other problems for such a simple explanation. The moment, which is the product of the magnitude and effective volume of coherent crustal magnetization, must be at least an order of magnitude greater than for crustal rocks on Earth. For strength of magnetization similar to terrestrial upper crust the depth of coherent magnetization would have to be ~30 km. This would require an exceedingly high rate of heat loss since the crust must cool to a temperature lower than the Curie temperature of the dominant magnetic mineral throughout this entire depth interval on a timescale shorter than the interval between reversals. Alternate explanations require an unusually high concentration of the magnetic minerals or an exceedingly vigorous convection leading to a very strong dynamo. *Acuña et al.* [1999] suggested an alternative to reversals of the dipole field. A thin, highly magnetized plate, broken into linear blocks and separated by injection of material of lower magnetism, would show a similar pattern of reversals in the radial magnetic field at the orbital altitude. However, at this point no fully satisfactory model is able to explain these new observations of the magnetic field.

Magnetic anomalies are not associated with the Argyre, Hellas, or Isidis basins, suggesting that the impact events that produced these features postdate the cessation of dynamo action. Furthermore, the linear magnetic pattern has been destroyed in the vicinity of Hellas, either through reheating above the Curie point or by mechanical destruction of the coherent magnetization. The 9 km of relief associated with the Hellas basin implies that the lithosphere at the time of its formation was of substantial thickness and possessed long-term strength. Since Hellas and its ejecta are extensively modified by cratering, the magnetic and topographic evidence both suggest that the crust in the southern hemisphere has cooled rapidly enough to achieve a substantial thickness prior to the end of heavy bombardment.

8.1.2. Geologic processes. Analyses of MOC data have shown that layered sequences of rock are much more common than previously thought in the upper crust of Mars [*Malin et al.*, 1998; *Malin and Edgett*, 2000b; *Malin and Edgett*, this issue]. A common view was that the northern plains region was covered with volcanic flows but that the heavily cratered highlands are a megabreccia of primordial crust. However, layered crust is exposed to a depth of almost 10 km on the walls of Valles Marineris, suggesting that thick sequences of volcanic rocks may be present within the southern hemisphere (Figure 8a). Further, the data show different thicknesses and types of layers across the planet, some with different albedo and some with different resistance to erosion [*Malin and Edgett*, this issue]. These characteristics suggest that layers are composed of volcanic tuffs, aeolian deposits, or both. Complex sequences of events and processes can be discerned in some images. For example, partially denuded craters reveal a period of impact into horizontal layers and subsequent cover by a thick friable layer that has now been partially removed, probably by aeolian activity and possibly at the present time (Figure 8b). Also, analysis of crater populations on high-resolution MOC images indicates that some lava flows within the Arsia Mons caldera may be as young as 40–100 million years [*Hartmann et al.*, 1999].

TES spectral data indicate that there are two somewhat different rock compositions, both basically basaltic, whose distribution can be spatially mapped in the low-albedo areas over the surface [*Bandfield et al.*, 2000; *Christensen et al.*, 2000b]. In general, andesitic compositions occur in the northern plains, and basaltic compositions occur in the southern highlands. In fact, these results are consistent with alpha proton X-ray spectrometer (APXS) analyses of rocks at the Pathfinder landing site and reanalysis of Viking Lander X-ray fluorescence spectrometer (XRFS) data [*Larsen et al.*, 2000]. The high-albedo areas provide nondiagnostic spectra similar to that of atmospheric dust. Analyses of TES infrared spectra also demonstrate for the first time the abundant presence of pyroxene and plagioclase feldspar, the low abundance or lack of quartz, and the absence of a pervasively weathered surface, at least in the darker areas. The landers have shown that the soils had high iron, sulfur, and chlorine and that the soil particles are strongly magnetic, probably owing to an iron pigment. The soils are commonly interpreted as secondary weathering products, such as smectite, of mafic igneous rocks, possibly owing to palagonization of basalt. However, a high abundance of weathering minerals is not confirmed by the remote-sensing observations. Spectral mapping has established a unique area, ~350 × 350 km along with several smaller nearby areas, that has abundant relatively coarse-grained hematite [*Christensen et al.*, 2000a, 2000c]. The presence of this material in a thin flat-lying layer suggests an aqueous origin. However, the search for carbonate, sulfate, or quartz-rich rocks has been fruitless despite careful analyses of many million spectra.

The MOC high-resolution images show an incredible array of depositional and erosional aeolian landforms, including dunes, sand sheets, and yardangs as well as a pervasive thin layer of surface dust. The nature and origin of neither the sand nor the dust is known. *Ruff and Christensen* [1999] have shown that infrared spectra for the bright and dark albedo patches on Mars are well matched by a fine and a coarse aggregate, respectively, of pyroxene and plagioclase. Thus the bright regions as well as the dark regions, and much of the soil and dust, may be simply basaltic material ground up by impact processes or physical weathering. The light colored dunes may simply consist of sand-sized aggregate particles. Albedo mapping shows that significant changes in the pattern of light and dark material have occurred since the Viking observations, indicative of current aeolian activity [*Jakosky and Mellon*, this issue; *Jakosky et al.*, 2000]. Both albedo and thermal inertia mapping are being carried to higher resolution as the mapping mission proceeds.

8.2. Climate

Major MGS science objectives are to address the volatile (carbon dioxide, water) and dust cycles and the Martian atmosphere over the course of a Mars year from the Sun-synchronous circular orbit. The term climate is used because the emphasis is on the seasonal variations rather than the daily variations of the atmosphere. However, the additional year spent in the elliptical orbit also allowed acquisition of atmospheric data at different times of day.

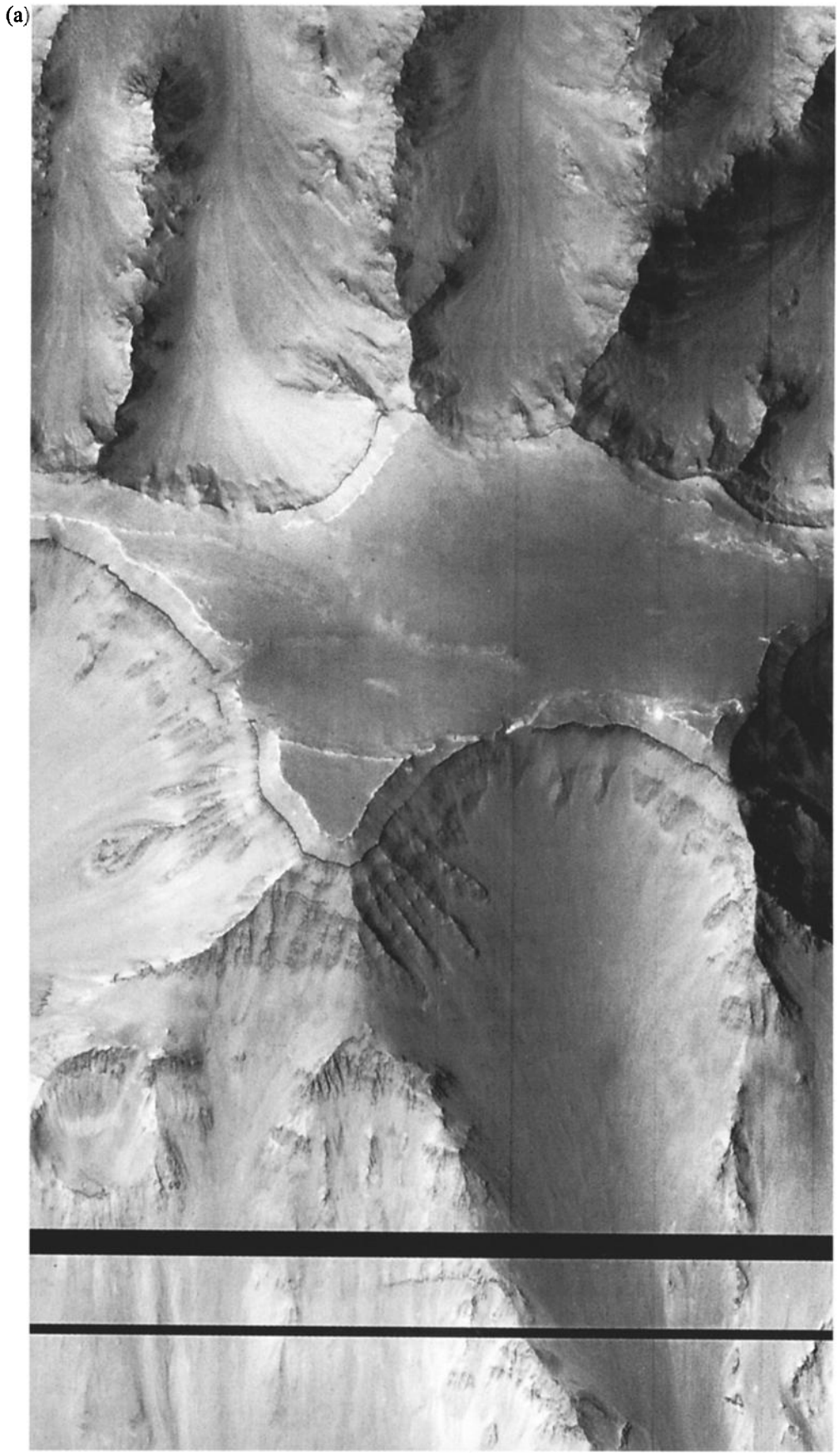

Figure 8. MOC images showing layering: (a) a thick layered sequence exposed in steep slopes surrounding a plateau within the Valles Marineris and (b) an exhumed crater within thinly layered deposits in Kasei Vallis.

Figure 8. (continued)

8.2.1. Structure and dynamics of the atmosphere. Although Earth and Mars have evolved atmospheres of very different compositions, it was predicted and has been shown that they have similar global circulation patterns [*Haberle*, 1986]. Both have atmospheres that are nearly transparent to sunlight and store almost no heat. Sunlight passes through the atmosphere without heating it and heats the surface, which then heats the atmosphere from below. The thin atmosphere and lack of oceans mean that temperature changes rapidly in response to diurnal and seasonal changes in solar input. Both planets have an obliquity that leads to significantly more heating of the surface in the tropics than in the poles; the resulting temperature gradient produces a pressure gradient that drives a north-south (meridional) circulation. The planets have a similar rotation rate, which determines the magnitude of the Coriolis force deflecting the moving air masses. Air rises where the solar heating is strongest and moves toward the poles and cools, sinking in the subtropics to form circulating cells (the Hadley cells). On Mars, in the absence of oceans, the rising branch closely follows the subsolar point, possibly as far as 25° from the equator, and probably leads to a single transequatorial Hadley cell during part of the year. The Coriolis force deflects the northern moving upper branch to the east (the westerlies) and deflects the equatorward moving lower branch to the west (the easterly trade winds).

At middle and high latitudes, winds are predominately from the west, both at the surface and aloft. A band of intense winds (the jet stream) blows in the upper atmosphere at an altitude of ~30–40 km. Nearer the surface, high- and low-pressure storm systems migrate eastward, their strong winds transporting heat toward the poles. These storms are more regular in their timing on Mars, probably owing to the more rapid response of the atmosphere to temperature perturbations. The strength of the jet stream depends on the latitudinal surface temperature gradient, which on Earth tends to be buffered by the oceans. However, on Mars the winter seasonal polar caps extend to the midlatitudes, and the high temperature contrast between carbon dioxide ice and adjacent soil leads to jet streams many times stronger than on Earth. However, in summer, when the ice cap recedes, the surface soil has a more uniform temperature, and the jet stream and the associated low-level storms dissipate.

The highly elliptical orbit of Mars means that its seasons are of unequal duration and intensity. Compared with the northern seasons, the southern spring and summer are short and hot and the fall and winter are long and cold. At perihelion, Mars receives ~40% more solar input than at aphelion; the difference for Earth is only ~3%. This asymmetry has influence on the structure and dynamics of the atmosphere, but it has major influence on the seasonal cycles of carbon dioxide, of dust, and of water. Mars is unique in that almost 25% of its atmosphere cycles in and out of the carbon dioxide ice polar caps each year, causing a like global variation in surface pressure. Owing to the longer fall and winter, the south polar ice cap grows larger than the north polar cap, reaching ~45° latitude.

Models of the general circulation of the atmosphere of Mars, like the preceeding description, have been developed by a number of groups. These numerical models have reached a high level of maturity, but they were based on surprisingly little data. For example, the single "classic," but incomplete, temperature profile from pole to pole is now replaced by thousands of TES infrared profiles that provide spatial and temporal coverage over most of the Martian year. MGS has now provided seasonal and spatial global plots of temperature, dusty content, cloud abundance, water vapor, and calculated thermal winds [*Smith et al.*, this issue (b)]. RS has provided hundreds of precise vertical profiles of temperature and pressure in the lower atmosphere [*Hinson et al.*, 1999].

Among other things, such data confirm the existence of cross-equatorial Hadley circulation during part of the year, as predicted by models. The numerical models typically utilized a fixed amount of dust uniformly distributed in the atmosphere to meet thermal constraints that required some direct warming of the atmosphere. More recent models have injected dust into the model at particular times and locations or under appropriate conditions of calculated surface stress. New data provide an intercomparison of atmospheric temperatures derived from ground-based millimeter, TES, and Viking data, providing data on seasonal and interannual variability of temperature and dust loading [*Clancy*, 1999; *Clancy et al.*, 2000; *Smith et al.*, this issue (b)]. MGS observations show that the atmosphere can change rapidly from warm and dusty to cool and clear [*Conrath et al.*, 2000]. As was expected, the atmosphere in the southern summer is relatively dusty and warm, but the northern summer is cooler than expected with abundant water ice clouds. It is now clear that the radiative effects of the very common water ice clouds, and of the carbon dioxide ice clouds seen in the polar regions, will have to be included in future modeling.

Observations during the aerobraking period of MGS have provided new insight into the physical processes connecting the upper and lower atmospheres of Mars [*Bougher and Keating*, 1999]. The period of MGS aerobraking witnessed the onset, rise, and decay of a regional dust storm in the southern hemisphere. Rapid heating and expansion of the lower hemisphere expanded faster than the actual increase in dust content. Accelerometer densities at 130 km increased by a factor of almost 3 over a 2- to 3-day period as the atmosphere expanded by 8 km. The decay of the effects of the storm took almost 2 months. Continued observations have led to the discovery of a complex density wave structure in the upper atmosphere.

Topography is a major boundary condition for global circulation models and critical for mesoscale models, and the MOLA altimetry data are being incorporated into those models. The large relief near the dichotomy boundary and in the Tharsis region affects the lower branch of the Hadley circulation cell and produces waves in the upper atmosphere. Detailed topography of both polar regions and of the Hellas and Argyre basins is facilitating an understanding through mesoscale models of the role of downslope winds in initiating dust storms. We can also expect that the detailed thermal inertia maps [*Jakosky and Mellon*, this issue], indicative of local differences in daily cooling and heating rates, will also be incorporated into the mesoscale models.

8.2.2. Seasonal cycles of carbon dioxide, water, and dust. The general circulation of the present Mars atmosphere couples together the seasonal cycles of carbon dioxide, water, and dust. Most obvious, of course, is the waxing and waning of the seasonal carbon dioxide ice caps as nearly a quarter of the atmosphere alternately precipitates and sublimates from the surface. The abundance of water in the atmosphere is closely coupled to the cycle of carbon dioxide. The maximum abundance of water occurs during summer over the north pole. The permanent (residual) water ice cap becomes a source of atmospheric water during the summer, when the seasonal carbon dioxide frost has sublimated away and exposed the water ice.

Viking observations suggested that water ice was not exposed at the southern ice cap in summer but that it remained covered by carbon dioxide frost. If so, it would be a water vapor sink growing at the expense of the northern cap. Whether or not the carbon dioxide ice cover survives every summer is not yet clear, but observations over the period of the Mars Surveyor Program should clarify this issue.

The permanent polar ice caps are the largest known reservoirs of water on Mars. Visually, the high-albedo southern cap appears smaller, but new topography indicates that ice, in part covered by dust, forms a tabular disc, extending from each pole to ~85° latitude with a relief of about 800–1000 m at the edge [*Smith et al.*, 1999b; *Zuber et al.*, 1998]. The similarity in topographic profiles and the comparative rheology of water ice and carbon dioxide ice suggest that both permanent caps consist predominantly of water ice. The permanent south polar cap is water ice rather than carbon dioxide ice as previously believed by many workers. However, TES thermal observations, like those of Viking, are currently consistent with a surface carbon dioxide frost cover in all seasons. Depending on certain assumptions, the northern cap has a volume of $1–2 \times 10^6$ km^3 [*Zuber et al.*, 1992], and the southern cap has a volume of $2–3 \times 10^6$ km^3 [*Smith et al.*, 1999b]. A large, but unknown, volume of water is stored as ground ice, and most models of the seasonal behavior of water include a substantial seasonal interchange of water between the regolith and the atmosphere. Widespread observations of low-lying water ice clouds seem to substantiate that model.

The dust cycle is very closely coupled to the general circulation because of the feedback between dust lifting and the intensity of circulation. Dust raised by the winds tends to intensify the winds in a feedback manner, because the dust absorbs solar radiation and heats the atmosphere directly. MGS showed that the onset of a dust storm in the southern hemisphere was observed within days as a marked pressure increase in the upper atmosphere of the northern hemisphere. Global dust storms occur predominantly during the southern spring and summer, when Mars is near perihelion, because that is when the heating of its atmosphere and the intensity of circulation are greatest. Viking measurements of the attenuation of sunlight suggested that the atmosphere never completely cleared of dust in contradiction to reasonable settling rates. However, MGS has shown that water ice clouds are abundant, contributing to the attenuation of sunlight, and in addition must play an important role in controlling the vertical abundance of dust.

An important finding of MGS is the extent to which aeolian processes have modified the surface [*Malin et al.*, 1998]. Almost everywhere one looks, there is evidence of atmosphere-surface interaction in the form of dunes, sand sheets, wind erosion features, and even active dust devils and small localized storms. In several places it has been shown that sand transport is occurring currently. In general, dust is not lofted directly (it requires very strong wind), but dust is probably injected into the air during saltation of sand-sized material. In the past our thinking might have attributed most surface accumulation of atmospheric dust to the slow settling of fine dust after great storms, but the role of small and regional dust storms (a continuum of scales) must now be considered. Models of surface stress using MOLA topography are being used to predict locations of evolving dust storms, and these predictions will have to be confirmed by visual observation. This approach should help to clarify some major questions: why is there not a global storm every year, and what shuts off the storm once it starts? What are the mechanisms and processes that determine whether a large local storm dies or whether it grows into a regional or even a planet-encircling storm?

The layering in the polar deposits provides evidence that settling of dust and ice is and has been an important process. It can be assumed that dust particles form nuclei for water and carbon dioxide ice precipitation at times, but the importance and timing of this process in the seasonal cycles of dust, water, and carbon dioxide is not clear. The high-albedo residual ice cap overlies layered deposits, thick stacks of alternating light and dark layers with individual bands extending down to the limit of resolution. High-resolution MOC images show an abundance of pitted features, different in the north and the south, and presumably formed by a sublimation process. Residual ice dominates near the pole, and layered deposits become more abundant away from the pole, within troughs that form the distinctive swirl pattern and as a continuous feature around the edge of the cap. The composition of the layers is uncertain; wide proportions of red dust, sand, ice, and void space have been suggested. Peripheral are circumpolar deposits, commonly mantled by dunes and sand sheets. Fretted features and the shapes of craters indicate that these deposits are also underlain by or contain abundant ice. MOLA topography indicates the presence of esker-like and kame-like features, suggesting that the edge of the disc of layered deposits represents the edge of a retreating ice cap, frozen in space as a relic (J. Head, oral communication, 2000).

8.2.3. Water on Mars. Water as vapor and solid, when not in the sunlight, can be present in the atmosphere and polar regions of Mars, but liquid water is not stable under present atmospheric conditions. Calculations indicate that ground ice should be stable throughout the much of the year in the mid-latitudes and over the entire year in the polar regions. Observations of patterned ground, from Viking and MOC, indicate the current or recent presence of ground ice in the soil. Abundant evidence has been presented to show that water also existed in the past in the form of ground ice and groundwater—at times catastrophically released—and possibly even as standing bodies of water [*Carr*, 1996]. The channels provide the most dramatic evidence for water on Mars; water emerged from the highlands subsurface, carved channels as it flowed downstream, and emptied into the northern lowlands, where the broad channels end abruptly, possibly debouching into a body of water. Less dramatic are the smaller valley networks, whose pattern suggested the possibility that they were formed by surface runoff from rainfall during a climatic period during which the atmosphere was dense enough and warm enough to stabilize liquid water.

MOLA topography and MOC images are permitting the detailed mapping of the sinuous networks of outflow channels and ephemeral lakes, their sources, and their final destination in a northern ocean [*Head et al.*, 1998; *Parker et al.*, 1989] (Figure 9). Eventually, these studies will lead to understanding the heat source and the volume of ice that had to be melted to provide the necessary water and the timing of these events in the various channels. As yet, specially targeted MOC images [*Malin and Edgett*, 1999] provide little evidence for the proposed shoreline of an extensive ocean [*Parker et al.*, 1993]. However, MOLA topography suggests the presence of a bench at constant altitude around the lowest parts of the northern plains [*Head et al.*, 1998]. Patterned ground and crater char-

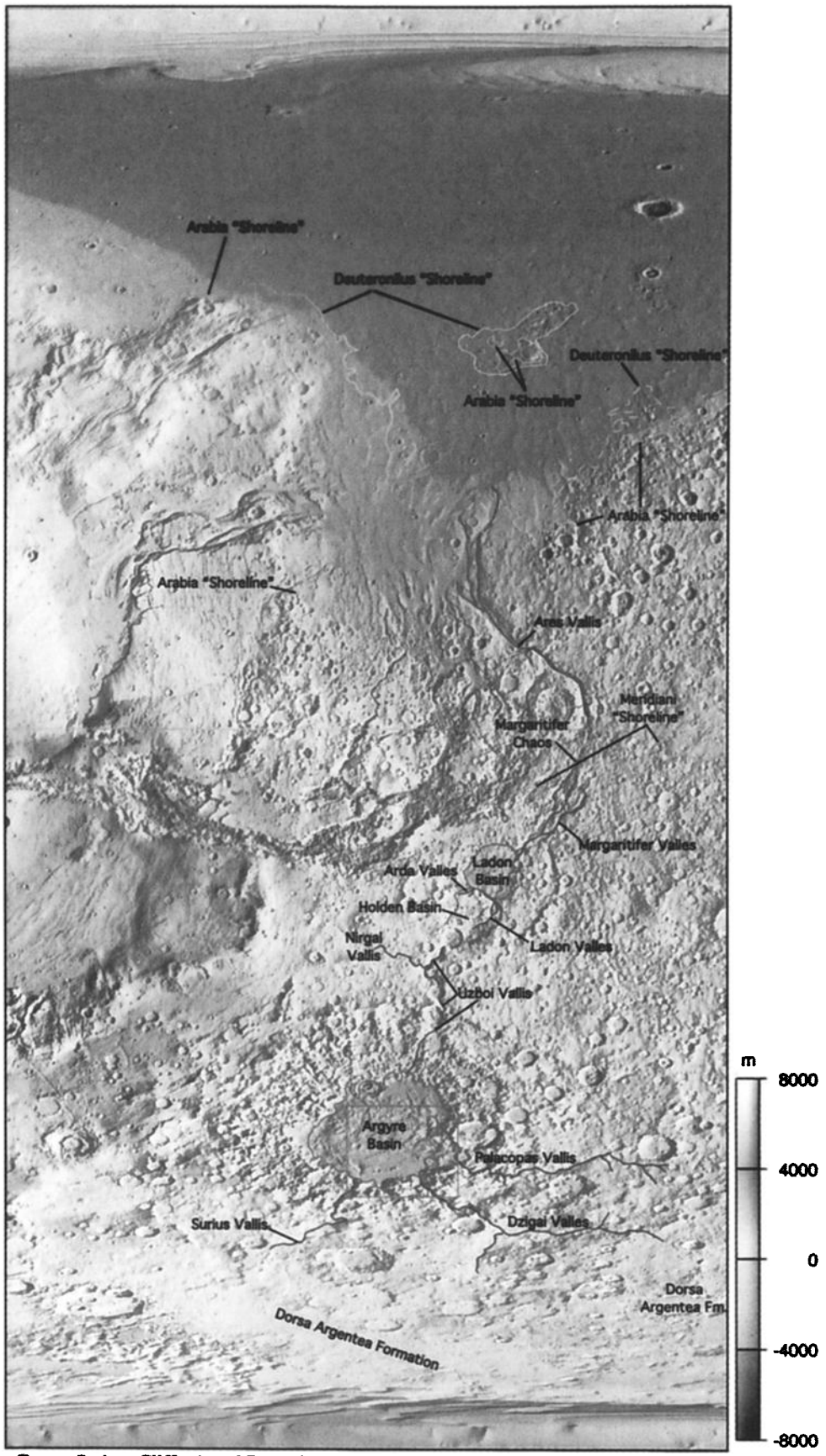

Figure 9. Networks of valleys and ephemeral lakes draining northward from Argyre Basin into the northern plains of Mars.

acteristics suggest the presence of ground ice within the northern plains, possibly residual from such a body of water.

The high-resolution MOC images have shown that the valley networks seen in the Viking images are typically not dissected with the hierarchy of tributaries characteristic of valley networks formed from surface runoff [*Malin and Carr*, 1999]. Instead, they terminate in stubby branches, typical of valley networks in regions of groundwater sapping or of thermokarst terrain. However, some MOC images do show sinuous patterns suggestive of sustained fluvial flow and erosion over a period of time, possibly under an ice cover. Moreover, high-resolution MOC images [*Malin and Edgett*, 2000a] show gullies on slopes suggestive of localized melting, seepage, and outflow of shallow ground ice.

It should be recognized that it took many years of study of the Viking and Mariner 9 images to achieve our current understanding of these complicated processes. It is clear that it will also take a long time to study the tremendous number of MOC images that have been and will be returned to Earth. The difference this time is that now all readers of this paper can quickly retrieve some of the more than 70,000 images for themselves from the Planetary Data System archives and make their own interpretations.

Despite the ambiguity in interpreting the valley networks, there still seems to have been an apparent change in the modification rate of craters early in Mars history near the end of the heavy bombardment. This observation retains the possibility of the current thinking, i.e., that for most of the period of heavy bombardment Mars was warm and wet and had a thick atmosphere and that toward the end of this period the atmosphere thinned greatly as carbon dioxide was removed and the surface cooled. Subsequently, perhaps for nearly 4 billion years, the Martian surface has been cold and dry, and aeolian action has been the dominant surface process. Clearly, the ongoing search for carbonate deposits on the surface, although so far fruitless, remains very important to the interpretation of the history of water on Mars.

It is generally understood that the presence of liquid water is critical to the evolution and retention of life. For this reason, NASA's Mars Program has identified the increase of our understanding of the history of water on Mars as its principal crosscutting and unifying theme. Many MGS observations are directed toward trying to identify places where liquid water might have existed in the past, e.g., shorelines, hot spring deposits, carbonate deposits, etc. Such areas would have a high priority for future sample return missions that would seek for evidence of past life on Mars. Evidence for localized groundwater seeps may be of great importance. However, in general, liquid water, derived from ground ice, has had an ephemeral presence in the present climate. Moreover, the new observations extend the period of cold and dry climate and do seem to push any warmer and wetter climate period further back into the early period of heavy bombardment. At this point we are a long way from understanding that critical period in Mars history. How did ground ice become widely distributed? Did it get recycled? Was it distributed in such abundance so as to provide sufficient water to carve all the outflow channels? Do the outflow channels represent flow of water under glacial ice during a period when most of Mars was covered by a thick ice sheet in a period even colder than today?

Because both Mars and Earth show evidence of drastic climate changes in the past, common mechanisms might be responsible (solar luminosity changes, orbital variations, volcanic eruptions, asteroid impacts, etc.). An improved understanding of climate change (with consequent effects on biological processes) may be the most important contribution of MGS to exobiologic science.

9. Summary

As of June 1, 2000, the Mars Global Surveyor spacecraft had completed over 14 months of operation (5500 orbits) of the planned 687-day Mars year of mapping. In addition, 1 year of aerobraking and science-phasing orbit observations also contributed to a unique and unexpected data set. Global maps of the topography, the gravity field, the magnetic field, the surface mineral composition and thermal inertia, the albedo, the atmosphere, and imaging have been obtained. In addition, high-resolution images have been obtained for ~0.1% of the planet. Whatever its future, Mars Global Surveyor has demonstrated that a single successful mission can reshape our understanding of a neighboring planet.

Note added at final submission: On February 1, 2001, at 1634 LT (Pacific Standard Time) MGS completed its 8505th orbit, marking the end of its primary mission, and embarked upon an extended mission. On June 2, 2001, at 2138 LT (Pacific Daylight Time) MGS completed orbit 10,000 with all instruments continuing to return data.

Acknowledgments. The research was carried out by the Mars Global Surveyor Project at the Jet Propulsion Laboratory, California Institute of Technology, under contract with the National Aeronautics and Space Administration. A.A. was Project Scientist, F.P. was Deputy Project Scientist, and T.T. was Science Manager and subsequently Mission Manager and Project Manager of the Project. R.E.A. was supported as a Mars Surveyor Program Interdisciplinary Scientist by JPL contract 1204044 to Washington University. The authors acknowledge the contribution of the entire project staff, including their colleagues at Lockheed Martin Aerospace and at all the home institutions of the instrument Principal Investigators and the Radio Science Team Leader. Many of the key project members and scientists were part of the early studies in 1981–1982 that led to Mars Observer and then to Mars Global Surveyor. Glenn Cunningham was project manager during the period from when Mars Observer was lost until the beginning of the mapping period. His contribution to the amazing success of MGS was outstanding; upon three occasions he made difficult decisions that preserved the scientific integrity of the mission. As spacecraft system manager throughout Mars Observer and MGS development, George Pace was always watchful for "creeping science requirements," but his selection of a larger HGA nearly doubled the capability for science downlink. Much of this work was drawn from a variety of project documents and we thank their authors, particularly Glenn Cunningham, Pat Esposito, Wayne Lee, and George Pace. Pat Esposito carefully checked the sections on mission and mission operations. We thank Pat Esposito, Wayne Lee, Mike Malin, Tim Parker, and Susan Slavney for help in figure and table generation.

References

Acton, C. H., Jr., The SPICE concept: An approach to providing geometric and other ancillary information needed for interpretation of data returned from space science instruments, in *Proceedings of the 2nd International Symposium on Space Information Systems*, pp. 1029–1035, Am. Inst. of Aeron. and Astron., New York, 1991.

Acuña, M. H., et al., The Mars Observer magnetic fields investigation, *J. Geophys. Res.*, *97*, 7799–7814, 1992.

Acuña, M. H., et al., Magnetic field and plasma observations at Mars: Initial results of the Mars Global Surveyor mission, *Science*, *279*, 1676–1680, 1998.

Acuña, M. H., et al., Global distribution of crustal magnetization discovered by the Mars Global Surveyor MAG/ER experiment, *Science*, *284*, 790–793, 1999.

Acuña, M. H., et al., Magnetic field of Mars: Summary of results from the aerobraking and mapping orbits, *J. Geophys. Res.*, this issue.

Albee, A. L., F. D. Palluconi, and R. E. Arvidson, Mars Observer Mission, *J. Geophys. Res.*, *97*, 7665–7680, 1992.

Albee, A. L., F. D. Palluconi, and R. E. Arvidson, Mars Global Surveyor Mission: Overview and status, *Science*, *279*, 1671–1672, 1998.

Bandfield, J. L., V. E. Hamilton, and P. R. Christensen, A global view of Martian surface compositions from MGS-TES, *Science*, *287*, 1626–1630, 2000.

Bills, B. G., and A. J. Ferrari, Mars topography, harmonics and geophysical implications, *J. Geophys. Res.*, *83*, 3497–3508, 1978.

Bougher, S. W., and G. M. Keating, Mars Global Surveyor aerobraking: Atmospheric trends and model interpretation, *Adv. Space Res.*, *23*(11), 1887–1897, 1999.

Butman, S., et al., The Mars Global Surveyor Ka-Band Experiment (MGS/KABLE-II), paper presented at 3rd Ka-Band Utilization Conference, Inst. Int. della Commun., Sorrento, Italy, 1997.

Caplinger, M. A., and M. C. Malin, Mars Orbiter Camera geodesy campaign, *J. Geophys. Res.*, this issue.

Carr, M. H., *Water on Mars*, 229 pp., Oxford Univ. Press, New York, 1996.

Christensen, P. R., et al., Thermal Emission Spectrometer experiment: The Mars Observer mission, *J. Geophys. Res.*, *97*, 7719–7734, 1992.

Christensen, P. R., et al., Detection of crystalline hematite mineralization on Mars by the thermal emission spectrometer: Evidence for near-surface water, *J. Geophys. Res.*, *105*, 9623–9642, 2000a.

Christensen, P. R., J. L. Bandfield, M. D. Smith, V. E. Hamilton, and R. N. Clark, Identification of a basaltic component on the Martian surface from Thermal Emission Spectrometer data, *J. Geophys. Res.*, *105*, 9609–9622, 2000b.

Christensen, P. R., M. C. Malin, R. V. Morris, J. Bandfield, M. Lane, and K. Edgett, The distribution of crystalline hematite on Mars from the Thermal Emission Spectrometer: Evidence for liquid water, *Proc. Lunar Planet. Sci. Conf. 31st*, p. 1627, 2000c.

Christensen, P. R., et al., Mars Global Surveyor Thermal Emission Spectrometer experiment: Investigation description and surface science results, *J. Geophys. Res.*, this issue.

Clancy, R. T., Orbital and interannual variability of the global Mars atmosphere, paper presented at Fifth International Conference on Mars, Lunar and Planet. Inst., Pasadena, Calif., 1999.

Clancy, R. T., B. J. Sandor, M. J. Wolff, P. R. Christensen, M. D. Smith, J. C. Pearl, B. J. Conrath, and R. J. Wilson, An intercomparison of ground-based millimeter, MGS TES, and Viking atmospheric temperature measurements: Seasonal and interannual variability of temperatures and dust loading in the global Mars atmosphere, *J. Geophys. Res.*, *105*, 9553–9572, 2000.

Connerney, J. E. P., M. H. Acuña, P. J. Wasilewski, N. F. Ness, H. Rème, C. Mazelle, D. Vignes, R. P. Lin, D. L. Mitchell, and P. A. Cloutier, Magnetic lineations in the ancient crust of Mars, *Science*, *284*, 794–798, 1999.

Conrath, B. J., J. C. Pearl, M. D. Smith, W. C. Maguire, P. R. Christensen, S. Dason, and M. S. Kaelberer, Mars Global Surveyor Thermal Emission Spectrometer (TES) observations: Atmospheric temperatures during aerobraking and science phasing, *J. Geophys. Res.*, *105*, 9509–9520, 2000.

Cunningham, G. E., Mars Global Surveyor Mission, 10 pp., Int. Astron. Fed., Paris, 1995.

Esposito, P., V. Alwar, S. Demcak, E. Graat, M. Johnston, and R. Mase, Mars Global Surveyor navigation and aerobraking at Mars, paper presented at 13th International Symposium on Space Flight Dynamics, Am. Astron. Soc., Goddard Space Flight Cent., Greenbelt, Md., 1998.

Esposito, P., V. Alwar, P. Burkhart, S. Demcak, E. Graat, M. Johnston, and B. Portock, Navigating Mars Global Surveyor through the Martian atmosphere: Aerobraking 2, paper presented at AAS/AIAA Astrodynamic Specialist Conference, Am. Astron. Soc., Girdwood, Alaska, Aug. 16–19, 1999.

Haberle, R. M., The climate of Mars, *Sci. Am.*, *254*, 54–62, 1986.

Hartmann, W. K., M. Malin, A. McEwen, M. Carr, L. Soderblom, P. Thomas, E. Danielson, P. James, and J. Veverka, Evidence for recent volcanism on Mars from crater counts, *Lett. Nature*, *397*, 586–589, 1999.

Head, J. W., III, M. Kreslavsky, H. Hiesinger, M. Ivanov, S. Pratt, N. Seibert, D. E. Smith, and M. T. Zuber, Oceans in the past history of Mars: Tests for their presence using Mars Orbiter Laser Altimeter (MOLA), *Geophys. Res. Lett.*, *25*, 4401–4404, 1998.

Hinson, D. P., R. A. Simpson, J. D. Twicken, G. L. Tyler, and F. M. Flasar, Initial results from radio occultation measurements with Mars Global Surveyor, *J. Geophys. Res.*, *104*(E11), 26,997–27,012, 1999.

Jakosky, B. M., and M. T. Mellon, High-resolution thermal inertia mapping of Mars: Sites of exobiological interest, *J. Geophys. Res.*, this issue.

Jakosky, B. M., M. T. Melton, H. H. Kieffer, P. R. Christensen, E. S. Varnes, and S. W. Lee, The thermal inertia of Mars from the Mars Global Surveyor Thermal Emission Spectrometer, *J. Geophys. Res.*, *105*, 9643–9652, 2000.

Johnston, M. D., P. B. Esposito, V. Alwar, S. W. Demcak, E. J. Graat, P. D. Burkhart, and B. M. Portock, The strategy for the second phase of aerobraking Mars Global Surveyor, in *AAS/AIAA Astrodynamics Specialist Conference*, 16 pp., AAS Publ. Off., San Diego, Calif., 1999.

Keating, G. M., et al., The structure of the upper atmosphere of Mars: In situ accelerometer measurements from Mars Global Surveyor, *Science*, *279*, 1672–1676, 1998.

Kieffer, H. H., B. M. Jakosky, C. W. Snyder, and M. S. Matthews (Eds.), *Mars*, Univ. of Ariz. Press, Tucson, 1992.

Larsen, K. W., R. E. Arvidson, B. L. Jolliff, and B. C. Clark, Correspondence and least squares analysis of soil and rock compositions for the Viking Lander 1 and Pathfinder landing sites, *J. Geophys. Res.*, *105*, 29,207–29,221, 2000.

Malin, M. C., and M. H. Carr, Groundwater formation of Martian valleys, *Nature*, *397*, 589–591, 1999.

Malin, M. C., and K. S. Edgett, Oceans or seas in the Martian northern lowlands: High resolution imaging tests of proposed coastlines, *Geophys. Res. Lett.*, *26*, 3049–3052, 1999.

Malin, M. C., and K. S. Edgett, Evidence for recent groundwater seepage and surface runoff on Mars, *Science*, *288*, 2330–2335, 2000a.

Malin, M. C., and K. S. Edgett, Sedimentary rocks of early Mars, *Science*, *290*, 1927–1937, 2000b.

Malin, M. C., and K. S. Edgett, Mars Global Surveyor Mars Orbiter Camera: Interplanetary cruise through primary mission, *J. Geophys. Res.*, this issue.

Malin, M. C., G. E. Danielson, A. P. Ingersoll, H. Masursky, J. Veverka, M. A. Ravine, and T. A. Soulanille, Mars Observer Camera, *J. Geophys. Res.*, *97*, 7699–7718, 1992.

Malin, M. C., et al., Early views of the Martian surface from the Mars Orbiter Camera of Mars Global Surveyor, *Science*, *279*, 1681–1685, 1998.

Martin, T. Z., Horizon Science Experiment for Mars Global Surveyor, *Bull. Am. Astron. Soc.*, *29*, 970, 1997.

Mitchell, D., Probing Mars' crustal magnetic field and ionosphere with the MGS Electron Reflectometer, *J. Geophys. Res.*, this issue.

Parker, T. J., R. S. Saunders, and D. M. Schneeberger, Transitional morphology in West Deuteronilus Mensae, Mars: Implications for modification of the lowland/highland boundary, *Icarus*, *82*, 111–145, 1989.

Parker, T. J., D. S. Gorsline, R. S. Saunders, and D. M. Schneeberger, Coastal geomorphology of the Martian northern plains, *J. Geophys. Res.*, *98*, 11,061–11,078, 1993.

Ruff, S. W., and P. R. Christensen, Thermal IR spectral characteristics of the Martian albedo features, paper presented at Fifth International Conference on Mars, Lunar and Planet. Inst., Pasadena, Calif., 1999.

Smith, D. E., W. L. Sjogren, G. L. Tyler, G. Balmino, F. G. Lemoine, and A. S. Konopliv, The gravity field of Mars: Results from Mars Global Surveyor, *Science*, *286*(5437), 4–97, 1999a.

Smith, D. E., et al., The global topography of Mars and implications for surface evolution, *Science*, *284*, 1495–1503, 1999b.

Smith, D. E., et al., Mars Orbiter Laser Altimeter (MOLA): Experiment summary after the first year of global mapping of Mars, *J. Geophys. Res.*, this issue (a).

Smith, M. D., J. C. Pearl, B. J. Conrath, and P. R. Christensen, Thermal Emission Spectrometer results: Mars atmospheric thermal structure and aerosol distribution, *J. Geophys. Res.*, this issue (b).

Solar System Exploration Committee, Planetary exploration through year 2000—A core program, NASA Adv. Counc., Washington, D. C., 1983.

Tyler, G. L., G. Balmino, D. P. Hinson, W. L. Sjogren, D. E. Smith, R. T. Woo, S. M. Asmar, M. J. Connally, C. L. Hamilton, and R. A. Simpson, Radio science investigations with Mars Observer, *J. Geophys. Res.*, *97*(E5), 7759–7779, 1992.

Tyler, G. L., G. Balmino, D. P. Hinson, W. J. Sjogren, D. E. Smith, R. A. Simpson, S. W. Asmar, P. Priest, and J. D. Twicken, Radio science observations with Mars Global Surveyor: Orbit insertion through one year in mapping orbit, *J. Geophys. Res.*, this issue.

Uphoff, C., Orbit selection for a Mars geoscience/climatology orbiter, paper presented at AIAA 22nd Aerospace Sciences Meeting, Am. Inst. of Aeron. and Astron., Reno, Nev., 1984.

Zuber, M. T., D. E. Smith, S. C. Solomon, D. O. Muhleman, J. W. Head, J. B. Garvin, J. B. Abshire, and J. L. Bufton, The Mars Observer Laser Altimeter investigation, *J. Geophys. Res.*, *97*, 7781–7798, 1992.

Zuber, M. T., et al., Observations of the north polar region of Mars from the Mars Orbiter Laser Altimeter, *Science*, *282*, 2053–2060, 1998.

A. A. Albee, Division of Geological and Planetary Sciences, California Institute of Technology, Mail Code 170-25, Pasadena, CA 91125. (aalbee@gps.caltech.edu)

R. E. Arvidson, McDonnell Center for Space Sciences, Department of Earth and Planetary Sciences, Washington University, St. Louis, MO 63130.

F. Palluconi and T. Thorpe, Jet Propulsion Laboratory, 4800 Oak Grove Drive, Pasadena, CA 91109.

(Received June 30, 2000; revised February 9, 2001;
accepted February 12, 2001.)